Meteorological Model Performance for Annual 2018 Simulation WRF v3.8

EPA-454/R-23-006
July 2023

Meteorological Model Performance for Annual 2018 Simulation WRF v3.8

U.S. Environmental Protection Agency
Office of Air Quality Planning and Standards
Air Quality Assessment Division
Research Triangle Park, NC

Meteorological Model Performance for Annual 2018 Simulation WRF v3.8

1. INTRODUCTION

The Weather Research and Forecasting model (WRF) was applied for the entire year of 2018 to generate meteorological data to support emissions and photochemical modeling applications for this year. The WRF meteorological fields will be converted to air quality modeling input data and used to support assessments of ozone, PM2.5, visibility, and a variety of toxics.

The WRF model was applied to the 12 km continental United States (12US) scale domain, initialized directly from meteorological analysis data. Model parameterizations and options outlined in this document were chosen based on a series of sensitivity runs performed by U.S. Environmental Protection Agency (USEPA) Office of Research and Development that provided an optimal configuration based on temperature, mixing ratio, and wind field. All WRF simulations were done by CSRA under contract to the USEPA.

2. MODEL CONFIGURATION

Version 3.8 of the WRF model, Advanced Research WRF (ARW) core (Skamarock, 2008) was used for generating the 2018 simulation. Selected physics options include Pleim-Xiu land surface model, Asymmetric Convective Model version 2 planetary boundary layer scheme, Kain-Fritsch cumulus parameterization utilizing the moisture-advection trigger (Ma and Tan, 2009), Morrison double moment microphysics, and RRTMG longwave and shortwave radiation schemes (Gilliam and Pleim, 2010).

The 12US WRF model was initialized using the 12km North American Model (12NAM) analysis product provided by National Climatic Data Center (NCDC). Where 12NAM data was unavailable, the 40km Eta Data Assimilation System (EDAS) analysis (ds609.2) from the National Center for Atmospheric Research (NCAR) was used. Analysis nudging for temperature, wind, and moisture was applied above the boundary layer only. The model simulations were conducted continuously. The 'ipxwrf' program was used to initialize deep soil moisture at the start of the run using a 10-day spinup period (Gilliam and Pleim, 2010). Landuse and land cover data were based on the 2011 National Land Cover Database (NLCD 2011)[1]. Sea surface temperatures were ingested from the Group for High Resolution Sea Surface Temperatures (GHRSST) (Stammer et al., 2003) 1km SST data.

Additionally, lightning data assimilation was utilized to suppress (force) deep convection where lightning is absent (present) in observational data. This method is described by Heath et al. (2016) and was employed to help improve precipitation estimates generated by the model.

[1] Subsequent review of the landuse data indicated that the data provided from NCAR had the incorrect byte allocation, resulting in slight differences of fractional landuse allocation. No significant performance degradation resulted from the use of this data.

Figures 2.1 shows the 12US domain, which utilized a Lambert conformal projection centered at (-97,40) with true latitudes of 33 and 45 degrees north. The 12US domain contains 412 cells in the X direction and 372 cells in the Y direction. The atmosphere is resolved with 35 vertical layers up to 50 mb (see table 2.1), with the thinnest layers being nearest the surface to better resolve the planetary boundary layer (PBL).

WRF Layer	Height (m)	Pressure (mb)	Sigma
35	17,556	5000	0.000
34	14,780	9750	0.050
33	12,822	14500	0.100
32	11,282	19250	0.150
31	10,002	24000	0.200
30	8,901	28750	0.250
29	7,932	33500	0.300
28	7,064	38250	0.350
27	6,275	43000	0.400
26	5,553	47750	0.450
25	4,885	52500	0.500
24	4,264	57250	0.550
23	3,683	62000	0.600
22	3,136	66750	0.650
21	2,619	71500	0.700
20	2,226	75300	0.740
19	1,941	78150	0.770
18	1,665	81000	0.800
17	1,485	82900	0.820
16	1,308	84800	0.840
15	1,134	86700	0.860
14	964	88600	0.880
13	797	90500	0.900
12	714	91450	0.910
11	632	92400	0.920
10	551	93350	0.930
9	470	94300	0.940
8	390	95250	0.950
7	311	96200	0.960
6	232	97150	0.970
5	154	98100	0.980
4	115	98575	0.985
3	77	99050	0.990
2	38	99525	0.995
1	19	99763	0.9975
Surface	0	100000	1.000

Table 2.1 WRF layers and their approximate height above ground level.

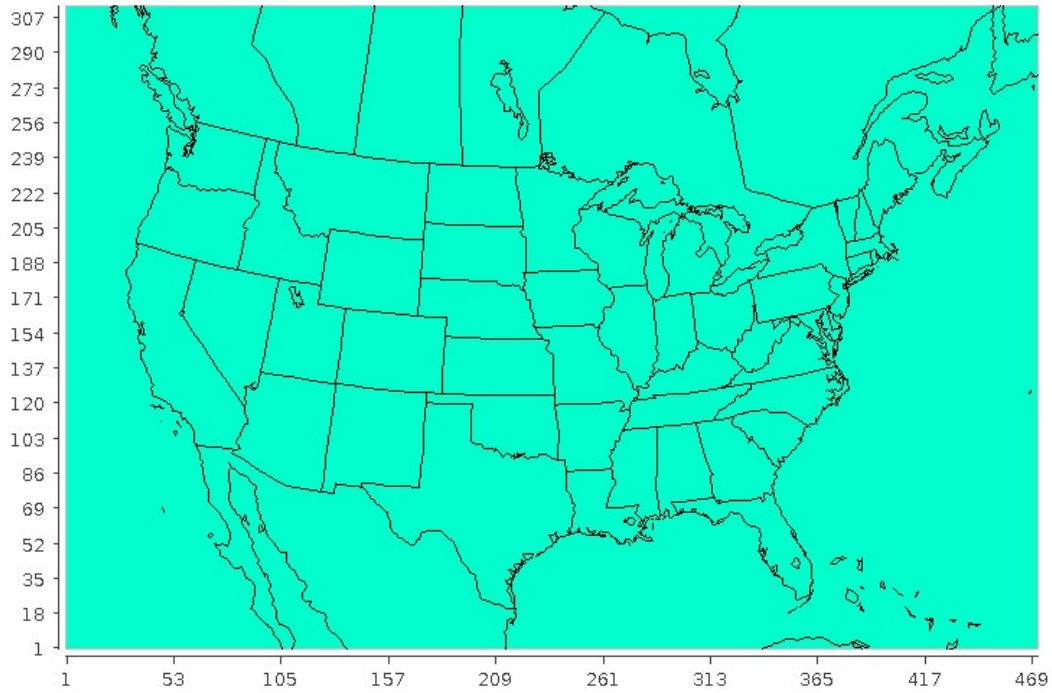

Figure 2.1 Map of WRF model domain: 12US.

3 MODEL PERFORMANCE DESCRIPTION

The WRF model simulations were evaluated to determine whether the output fields represent a reasonable approximation of the actual meteorology that occurred during the modeling period. Identifying and quantifying these output fields allows for a downstream assessment of how the air quality modeling results are impacted by the meteorological data. For the purposes of this assessment, 2-meter temperature and mixing ratio, 10-meter wind speed and direction, and shortwave radiation are quantitatively evaluated. A qualitative and quantitative evaluation of precipitation is also provided.

The observation database for surface-based temperature, wind speed and direction, and mixing ratio is based on measurements made at United States (i.e., National Weather Service) and Canadian (i.e., Environment Canada) airports. The observational dataset (ds472 network) is available from NCAR. Monitors used for evaluation are shown in Figure 3.1.

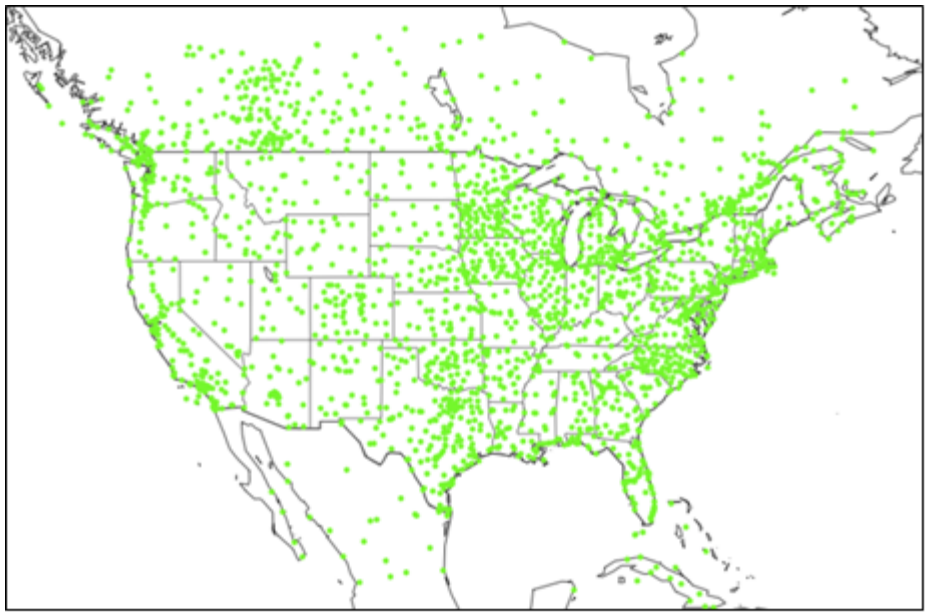

Figure 3.1 Stations used for model performance: ds472 network.

Shortwave downward radiation measurements are taken at surface-based monitor locations and this data is obtained through the Baseline Surface Radiation Network (BSRN, https://bsrn.awi.de/). This network is global and a map of the locations used in this evaluation is shown below (see Figure 3.2).

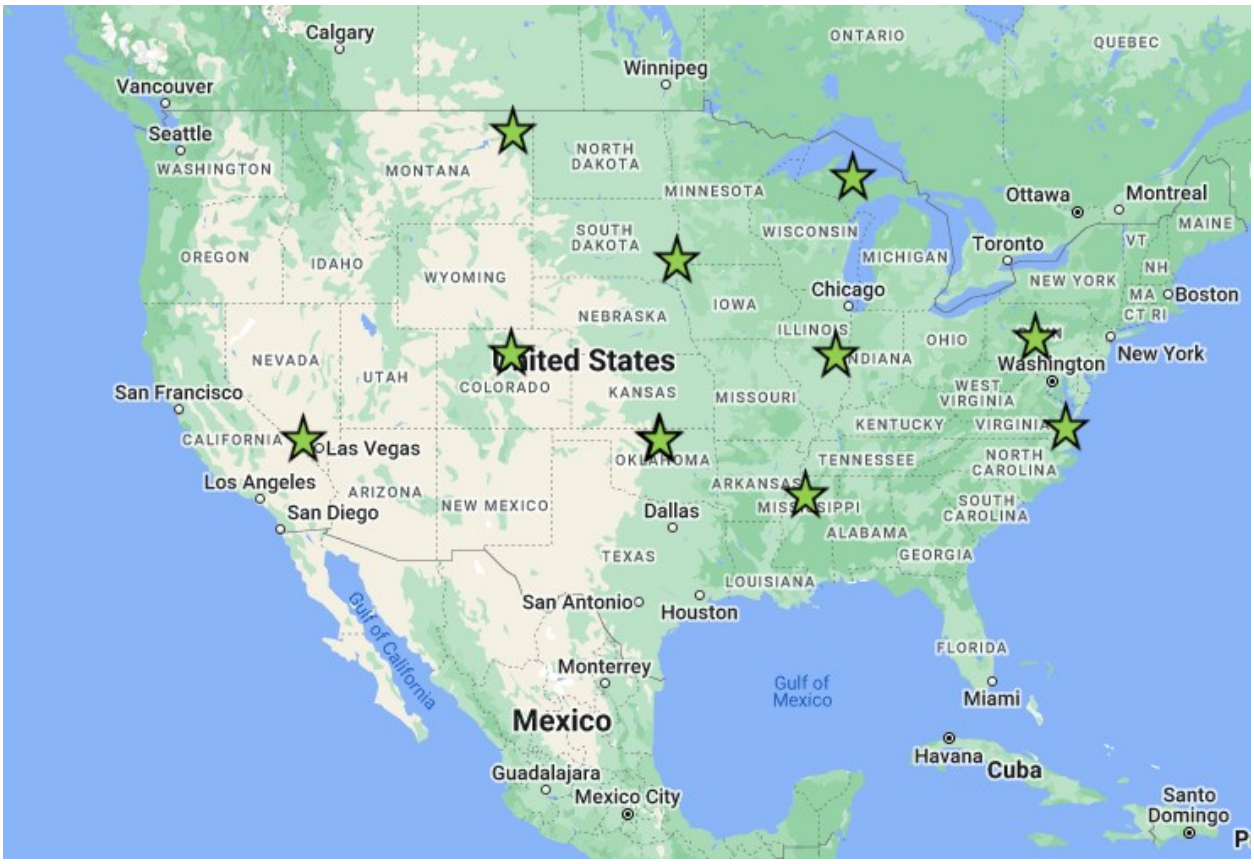

Figure 3.2. Location of radiation monitors.

Rainfall amounts are estimated by the Parameter-elevation Relationships on Independent Slopes Model (PRISM) model, which uses an elevation-based regression model to analyze precipitation. PRISM's horizontal resolution is approximately 2 to 4 km and is re-projected to the WRF modeling domain for direct comparison to model estimates. The rainfall analysis is limited to the contiguous United States as the model utilizes elevation and measured precipitation data at automated weather stations.

Model performance (i.e., temperature, wind speed, and mixing ratio) is described using quantitative metrics: mean bias, mean (gross) error, fractional bias, and fractional error (Boylan and Russell, 2006). These metrics are useful because they describe model performance in the measured units of the meteorological variable and as a normalized percentage. Since wind direction is reported in compass degrees, estimating performance metrics for wind direction is problematic as modeled and observed northerly winds may be similar but differences would result in a very large artificial bias. For example, the absolute difference in a northerly wind direction measured in compass degrees of 1° and 359° is 358° when the actual difference is only 2°. To address this issue, wind field displacement, or the difference in the U and V vectors between modeled (M) and observed (O) values, is used to assess wind vector performance (Equation 1). Performance is best when these metrics approach 0.

(1) Wind displacement (km) = $(\mathbf{U}_M - \mathbf{U}_O + \mathbf{V}_M - \mathbf{V}_O)$*(1 km/1000 m)*(3600 s/hr)*(1 hr)

Rainfall performance is examined spatially using side-by-side comparisons of monthly total rainfall plots. The WRF model outputs predictions approximately 15 meters above the surface while observations are at 10 meters. WRF generates output at near instantaneous values (90 second time step) as opposed to longer averaging times taken at monitor stations. This should be considered when interpreting model performance metrics.

3.1 Model Performance for Winds

WRF-predicted wind speed estimates are compared to surface-based measurements made in the ds472 network described earlier and shown below in Figure 3.1.1. Regional analysis of statistical metrics for wind speed performance by quarter[2] is shown in Table 3.1.1.

Statistically, WRF appears to perform very well for wind speed as the median value for the bias is centered around zero for all hours of the day and months of the year. However, there is a noticeable pattern in the performance when we examine wind speeds on a spatial scale (Figures 3.1.2-3.1.5).

In general, WRF slightly overpredicts (0.25 to 0.5 m/s) across much of the eastern US. Conversely, WRF tends to underpredict (-0.25 to -1 m/s) wind speeds in the western US, which persists across much of the year. As noted above, these biases generally persist regardless of changes in season.

[2] Quarters are Q1 (January, February, March), Q2 (April, May, June), Q3 (July, August, September), and Q4 (October, November, December).

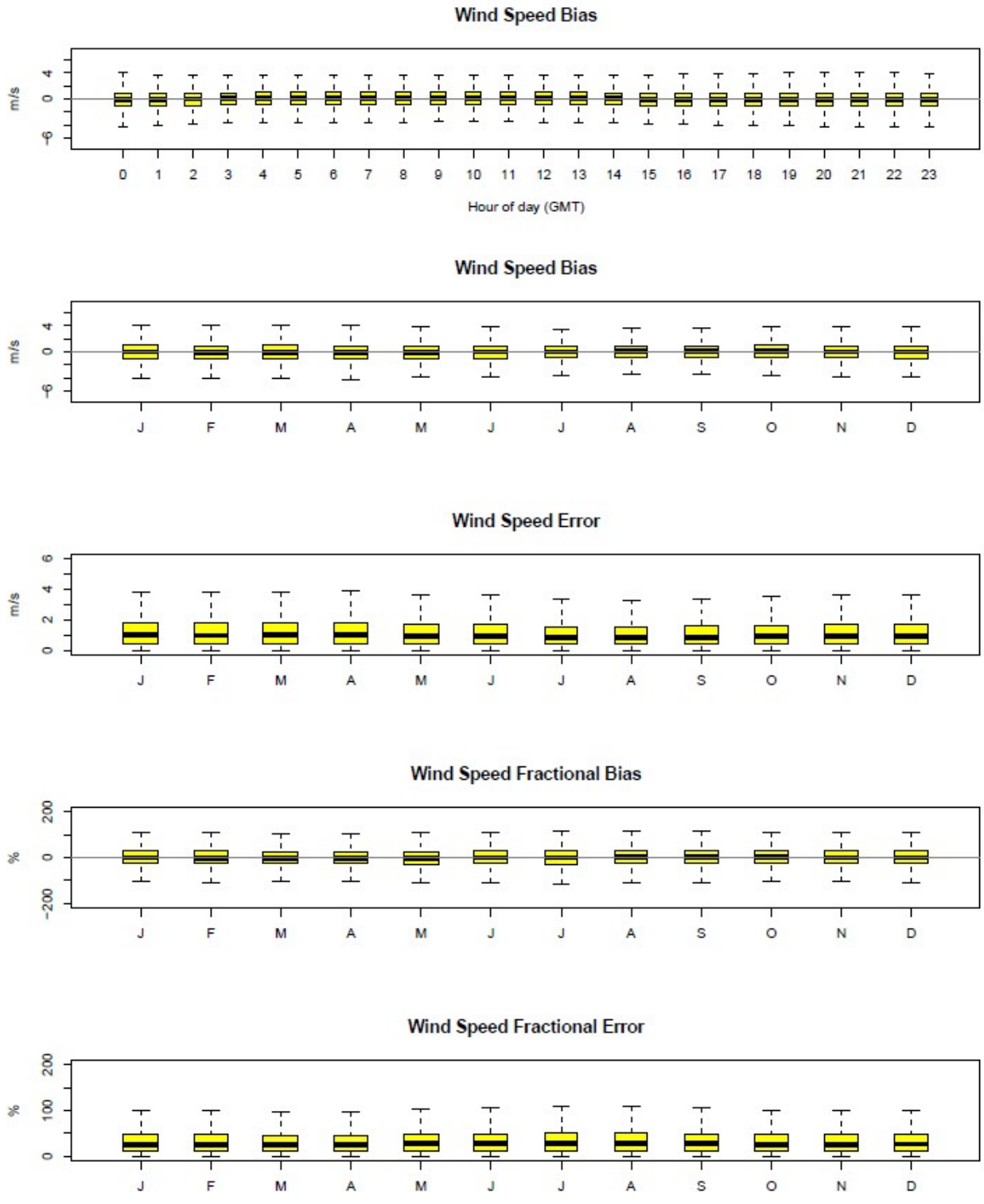

Figure 3.1.1. Distribution of hourly bias by hour and hourly bias, error, fractional bias, and fractional error for wind speed by month for 12US domain.

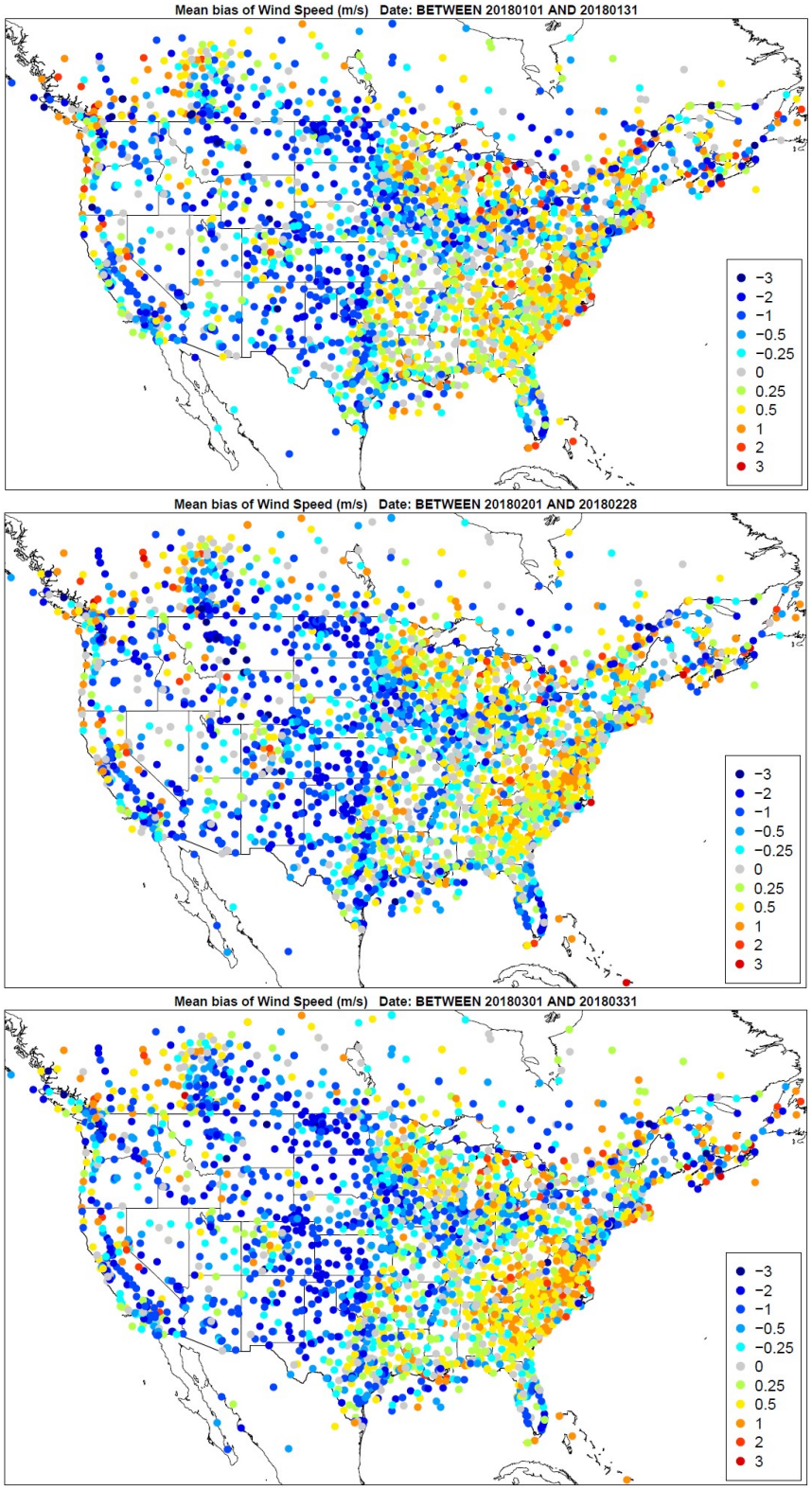

Figure 3.1.2. Spatial distribution of wind speed bias (m/s) across all hours for the months of January, February, and March (top to bottom).

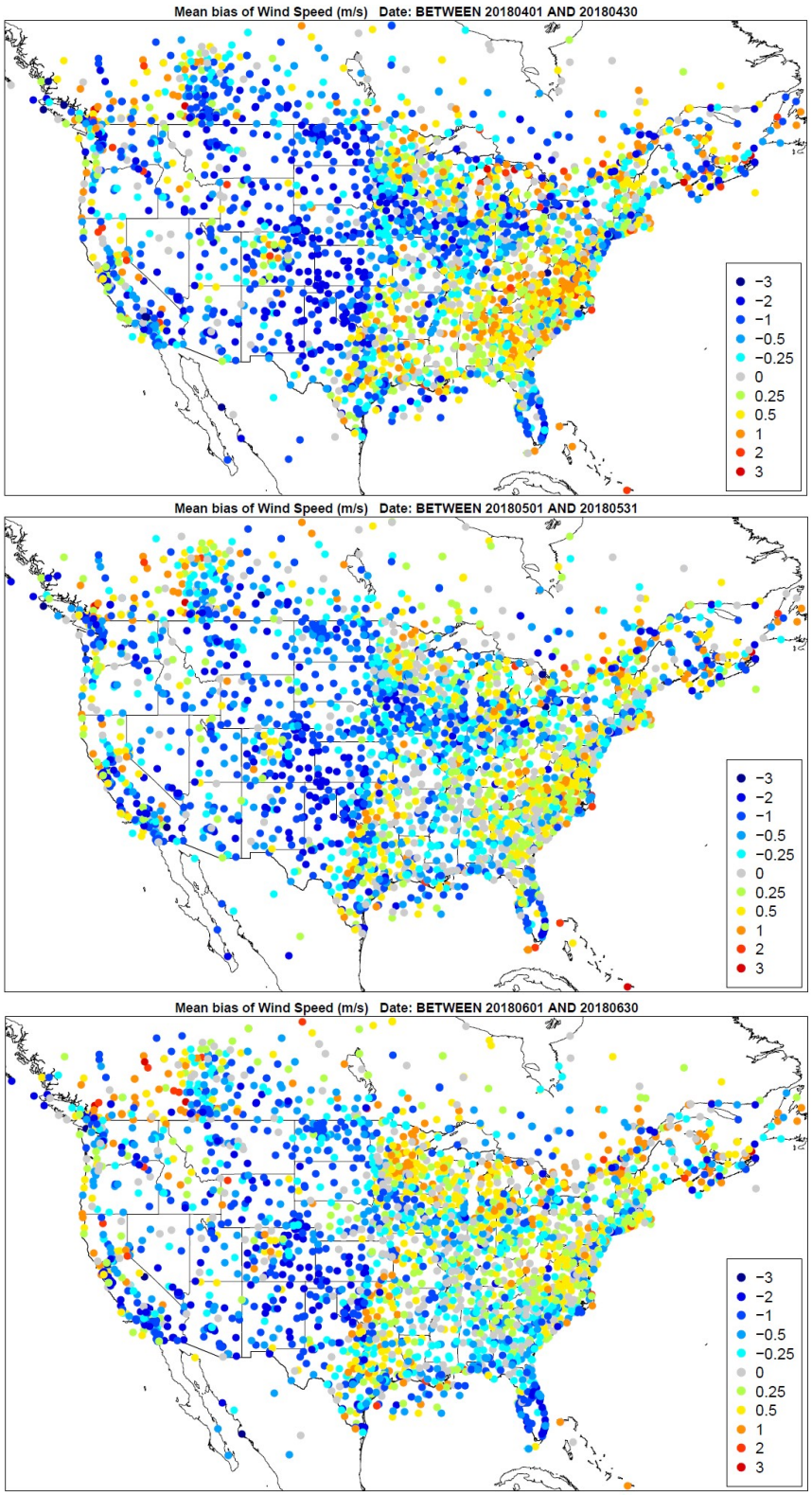

Figure 3.1.3. Spatial distribution of wind speed bias (m/s) across all hours for the months of April, May, and June (top to bottom).

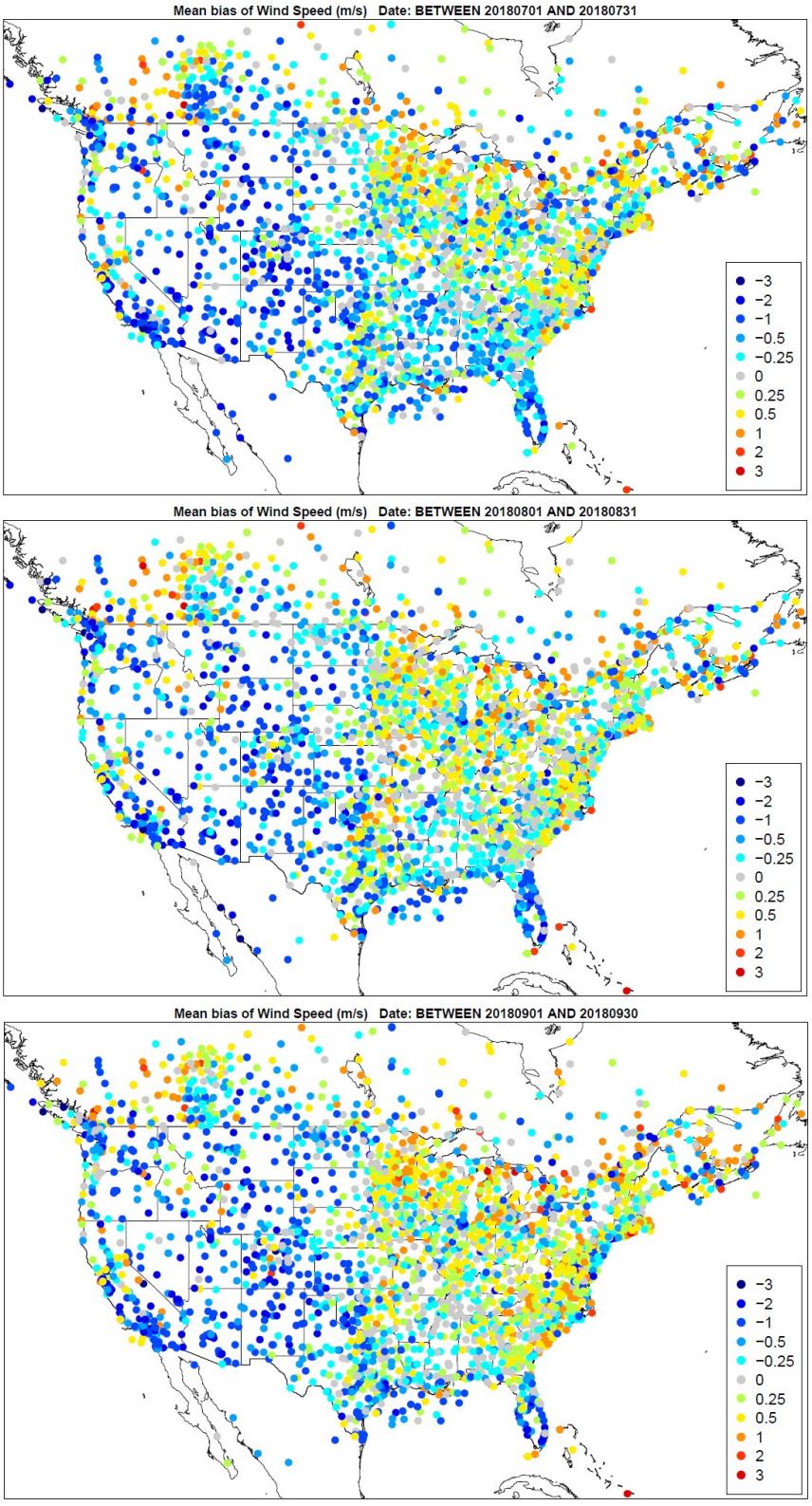

Figure 3.1.4. Spatial distribution of wind speed bias (m/s) across all hours for the months of July, August, and September (top to bottom).

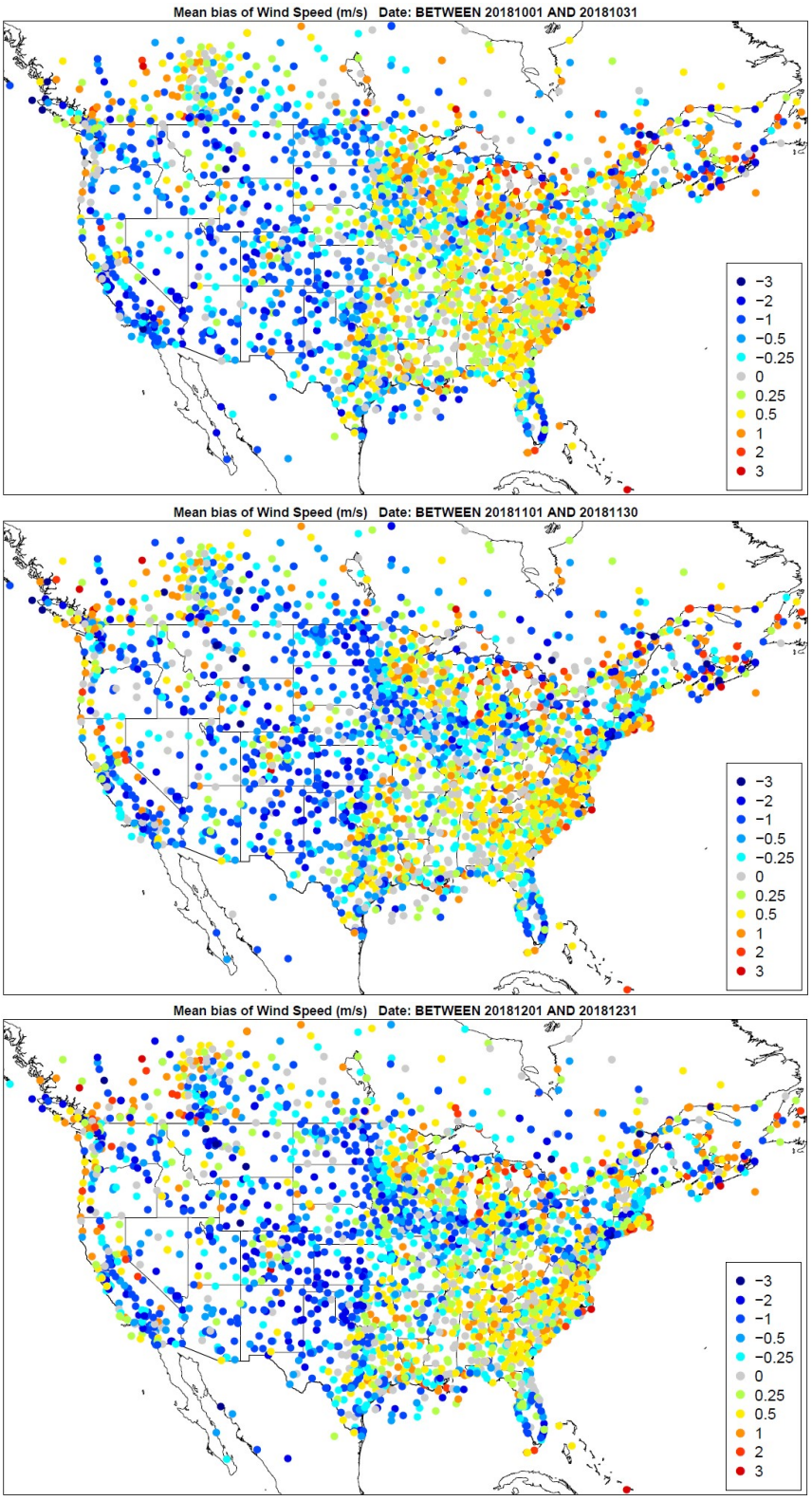

Figure 3.1.5. Spatial distribution of wind speed bias (m/s) across all hours for the months of October, November, and December (top to bottom).

Climate Region	Season	Mean Obs	Mean Mod	MAE	MB	NMB	NME	RMSE
Northeast	Q1	4.49	4.2	1.34	0.08	1.86	29.88	1.9
	Q2	3.89	3.49	1.18	-0.02	-0.58	30.38	1.7
	Q3	3.45	3.08	1.07	0.02	0.61	30.84	1.53
	Q4	4.14	3.75	1.29	0.06	1.46	31.21	1.85
N. Rockies & Plains	Q1	5.04	4.12	1.46	-0.7	-13.8	28.94	1.99
	Q2	4.93	4.14	1.42	-0.57	-11.5	28.76	1.93
	Q3	4.21	3.64	1.24	-0.33	-7.95	29.38	1.68
	Q4	4.77	4.04	1.32	-0.48	-10.08	27.61	1.79
Northwest	Q1	4	3.29	1.42	-0.4	-9.9	35.52	1.89
	Q2	4.01	3.35	1.32	-0.35	-8.64	32.95	1.75
	Q3	3.61	2.94	1.17	-0.38	-10.48	32.37	1.53
	Q4	3.63	2.93	1.32	-0.35	-9.59	36.41	1.77
Ohio Valley	Q1	4.46	4.12	1.12	-0.06	-1.32	25.02	1.54
	Q2	3.97	3.49	1.09	-0.13	-3.2	27.38	1.48
	Q3	3.23	2.89	0.92	0.04	1.18	28.48	1.24
	Q4	3.95	3.63	1.01	0.02	0.58	25.58	1.38
South	Q1	4.77	4.18	1.23	-0.33	-6.85	25.69	1.65
	Q2	4.76	4.13	1.24	-0.28	-5.92	26.03	1.68
	Q3	3.77	3.21	1.06	-0.23	-6.05	28.23	1.45
	Q4	4.3	3.81	1.11	-0.17	-3.86	25.69	1.49
Southeast	Q1	3.88	3.78	1.21	0.32	8.3	31.12	1.63
	Q2	3.48	3.12	1.1	0.07	2.12	31.61	1.47
	Q3	3.05	2.59	1.02	-0.04	-1.26	33.39	1.4
	Q4	3.51	3.27	1.13	0.27	7.59	32.19	1.55
Southwest	Q1	4.57	3.66	1.62	-0.61	-13.28	35.49	2.25
	Q2	4.88	3.99	1.63	-0.63	-12.91	33.45	2.2
	Q3	4.02	3.15	1.53	-0.68	-16.88	38.01	2.08
	Q4	4.01	3.18	1.45	-0.58	-14.4	36.25	2.01
Upper Midwest	Q1	4.5	4.26	1.14	0.05	1.19	25.34	1.55
	Q2	4.18	3.85	1.17	0.01	0.35	27.94	1.57
	Q3	3.59	3.47	1.07	0.28	7.89	29.82	1.44
	Q4	4.22	4.06	1.11	0.16	3.86	26.35	1.49
West	Q1	3.78	3.06	1.34	-0.35	-9.23	35.39	1.8
	Q2	4.34	3.6	1.36	-0.41	-9.4	31.27	1.81
	Q3	3.84	3.05	1.25	-0.5	-13	32.59	1.66
	Q4	3.53	2.78	1.29	-0.41	-11.67	36.43	1.74

Table 3.1.1. Mean observed, mean modeled, mean absolute error (MAE), mean bias (MB), normalized mean bias (NMB), normalized mean error (NME), and root mean square error (RMSE) for wind speed (m/s).

Wind vector displacement (km) is presented below (Figure 3.1.6) utilizing the ds472 observation network described earlier. These plots show the entire distribution of hourly wind displacement by month and by hour of the day. Overall, model performance is adequate in terms of wind vector differences. The average wind displacement for the WRF simulation is around 5km for all months and hours of the day. The interquartile ranges are roughly 2-10km. As the displacement is generally less than the resolution of the model, minimal impacts due to displacement of wind vectors are expected.

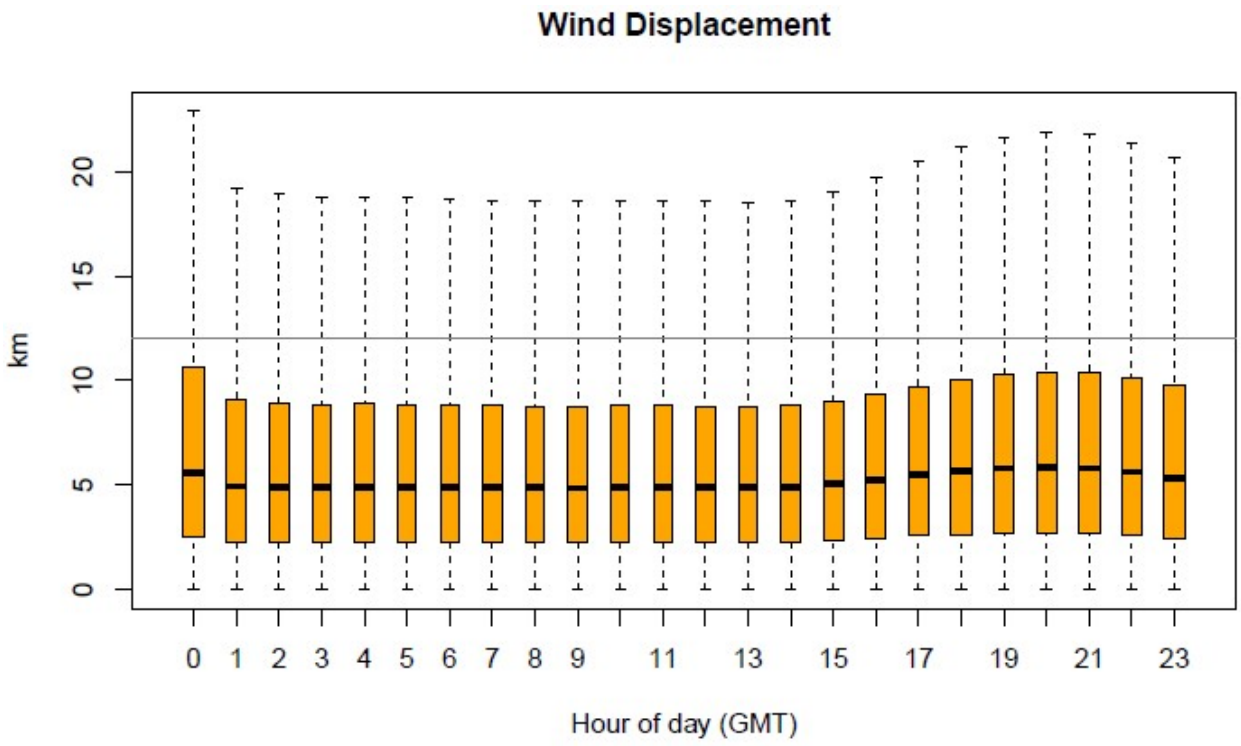

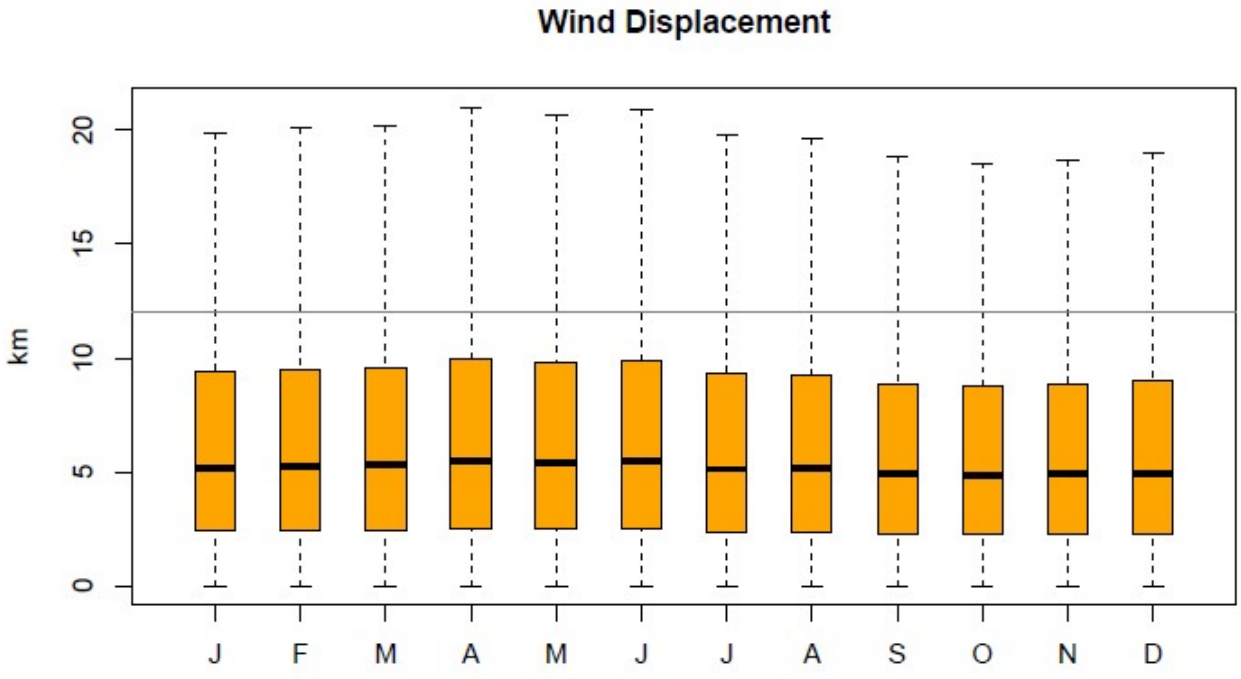

Figure 3.1.6. Distribution of hourly wind displacement by hour and month.

3.2 Temperature

Temperature estimates are compared to the ds472 observation network described earlier and are presented below (Figure 3.2.1). Regional analysis of statistical metrics for temperature performance by quarter is shown in Table 3.2.1.

WRF performs very well in terms of predicting temperature, showing a bias that oscillates around 0 degrees for most hours of the day and months of the year. Model error decreases noticeably during the Spring and Summer months. In general, the IQR of the bias of +/- 1 degree is acceptable model performance at this scale.

In Figures 3.2.3-3.2.6, spatial distribution of monthly biases is presented across all hours. WRF generally underpredicts temperatures slightly across the eastern US during the Winter into the early Spring with the undeprediction persisting longest in the northeast. A more noticeable overprediction is noted across the eastern US during from June through October with an average overprediction of 1 degree. In areas of the western US, performance for temperature is mixed, with persistent significant overpredictions and underpredictions observed in varying locations.

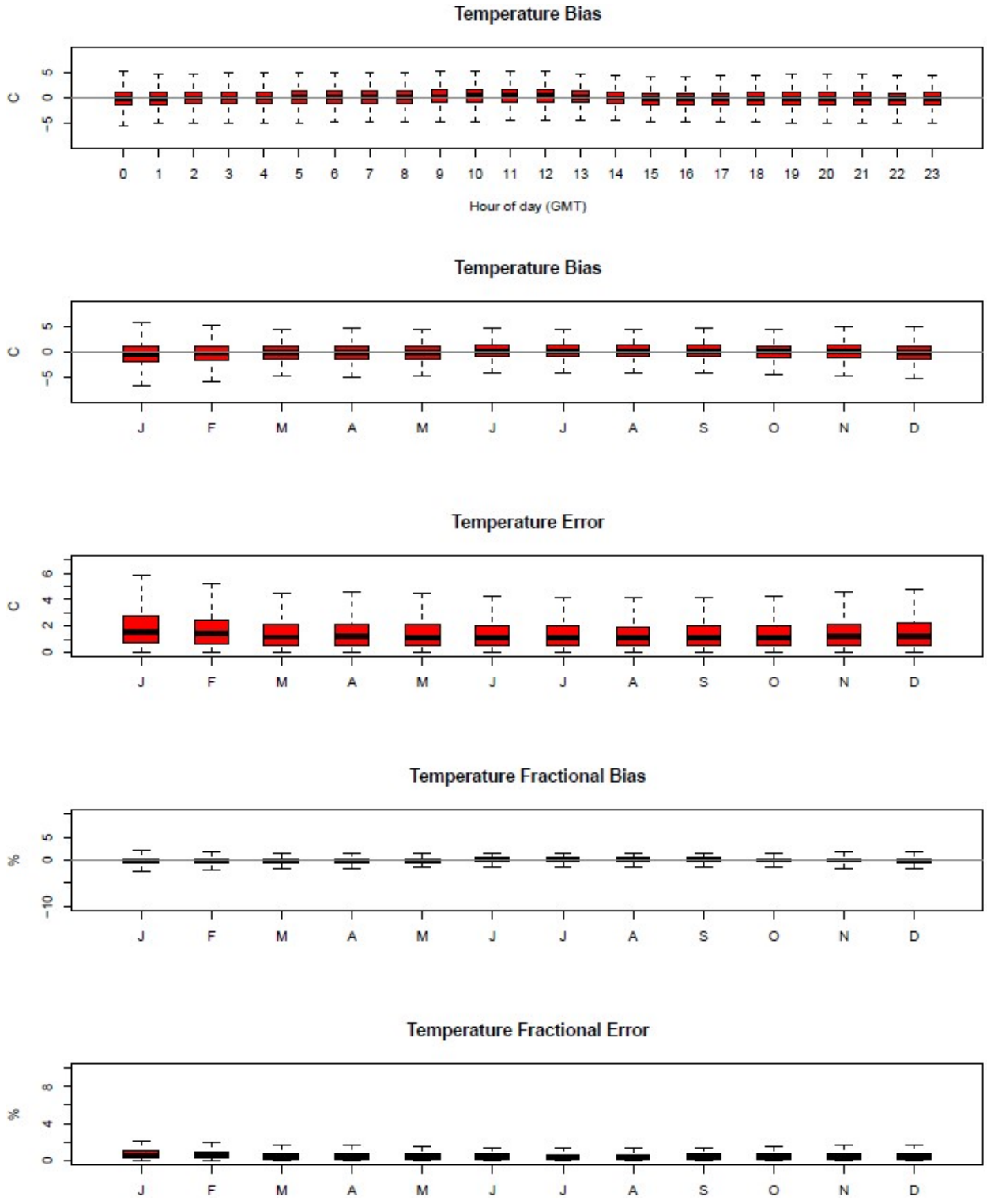

Figure 3.2.1. Distribution of hourly bias by hour and hourly bias, error, fractional bias, and fractional error for temperature by month.

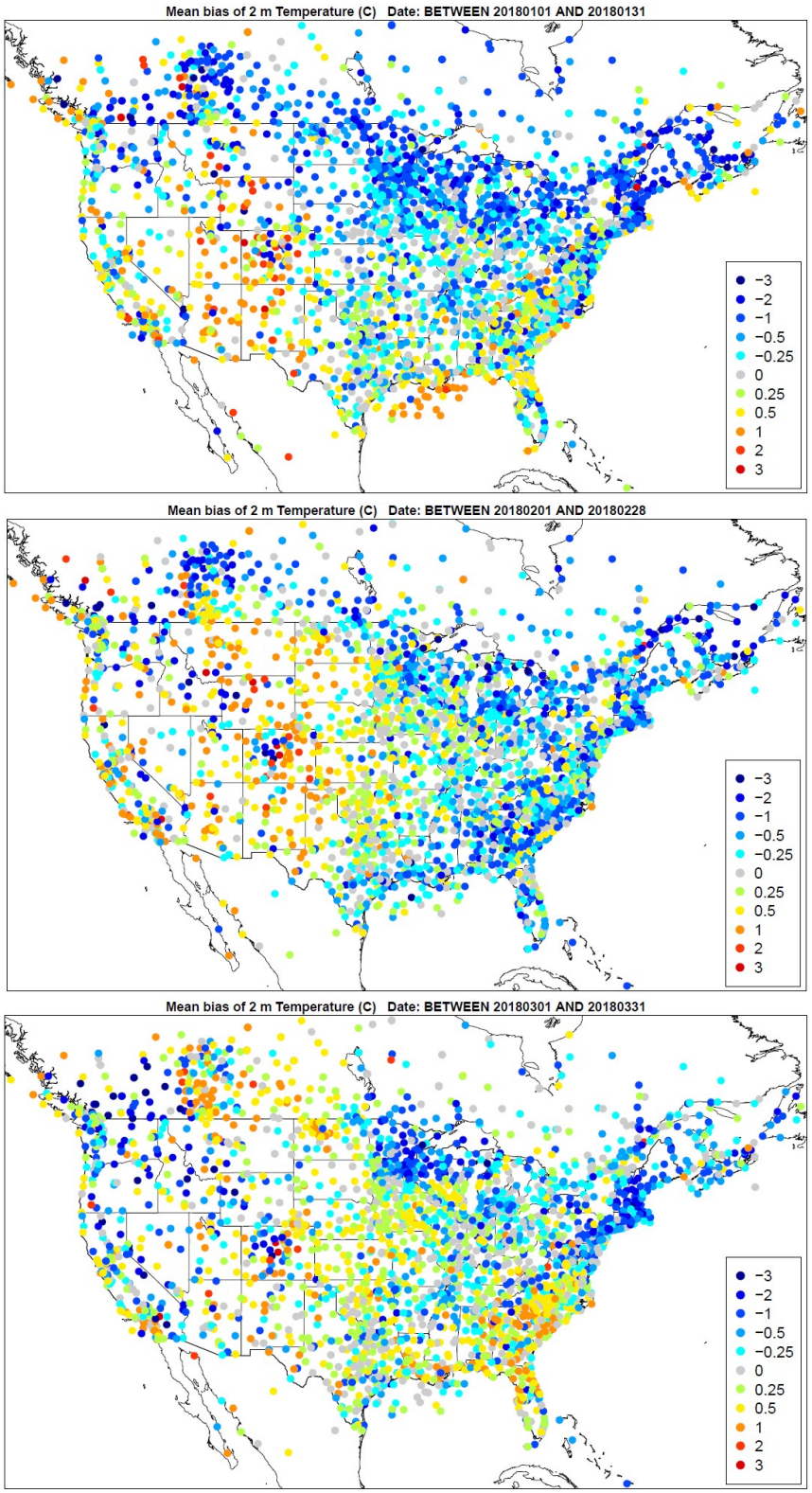

Figure 3.2.2. Spatial distribution of temperature bias (C) across all hours for the months of January, February, and March (top to bottom).

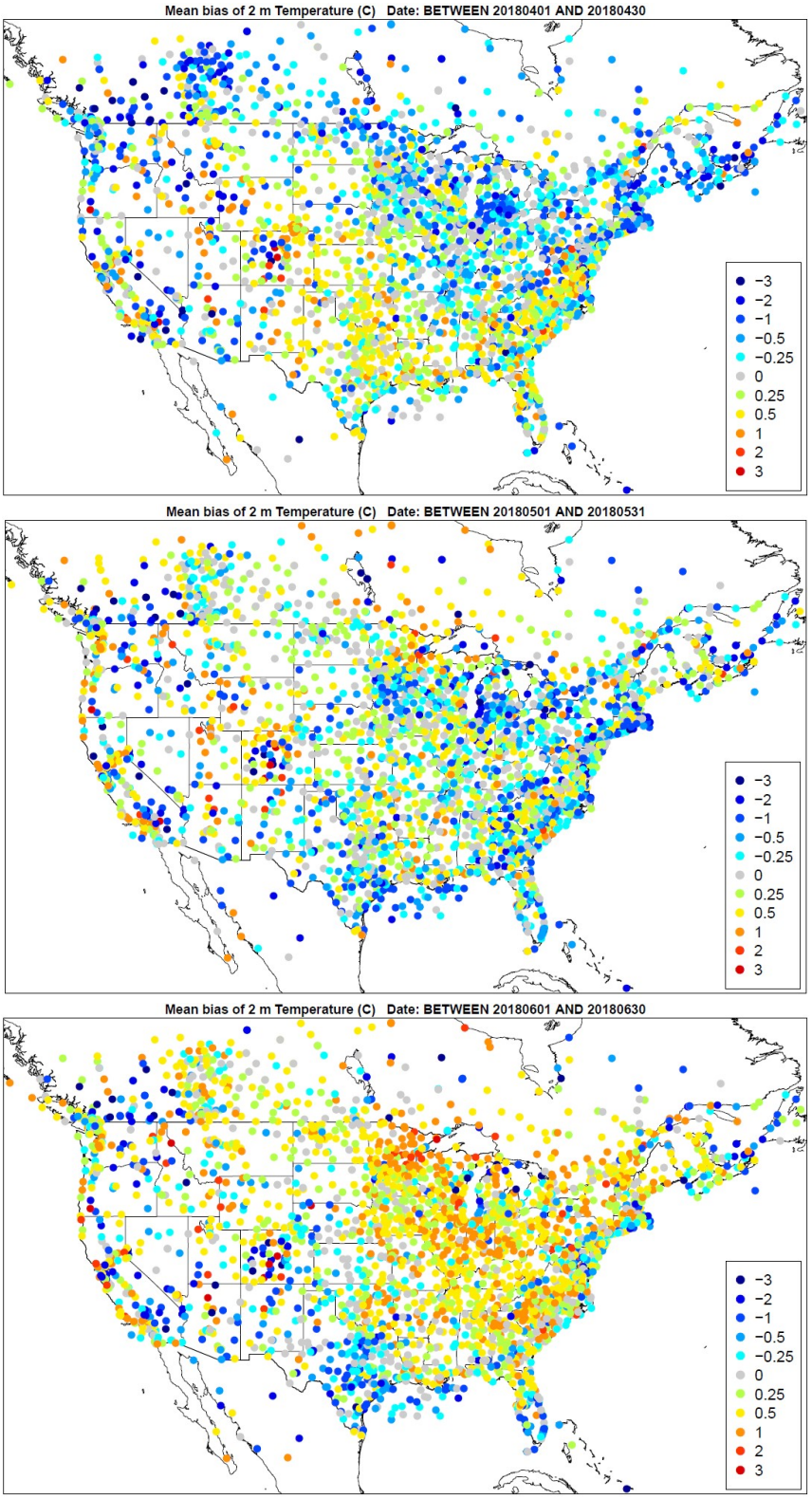

Figure 3.2.3. Spatial distribution of temperature bias (C) across all hours for the months of April, May, and June (top to bottom).

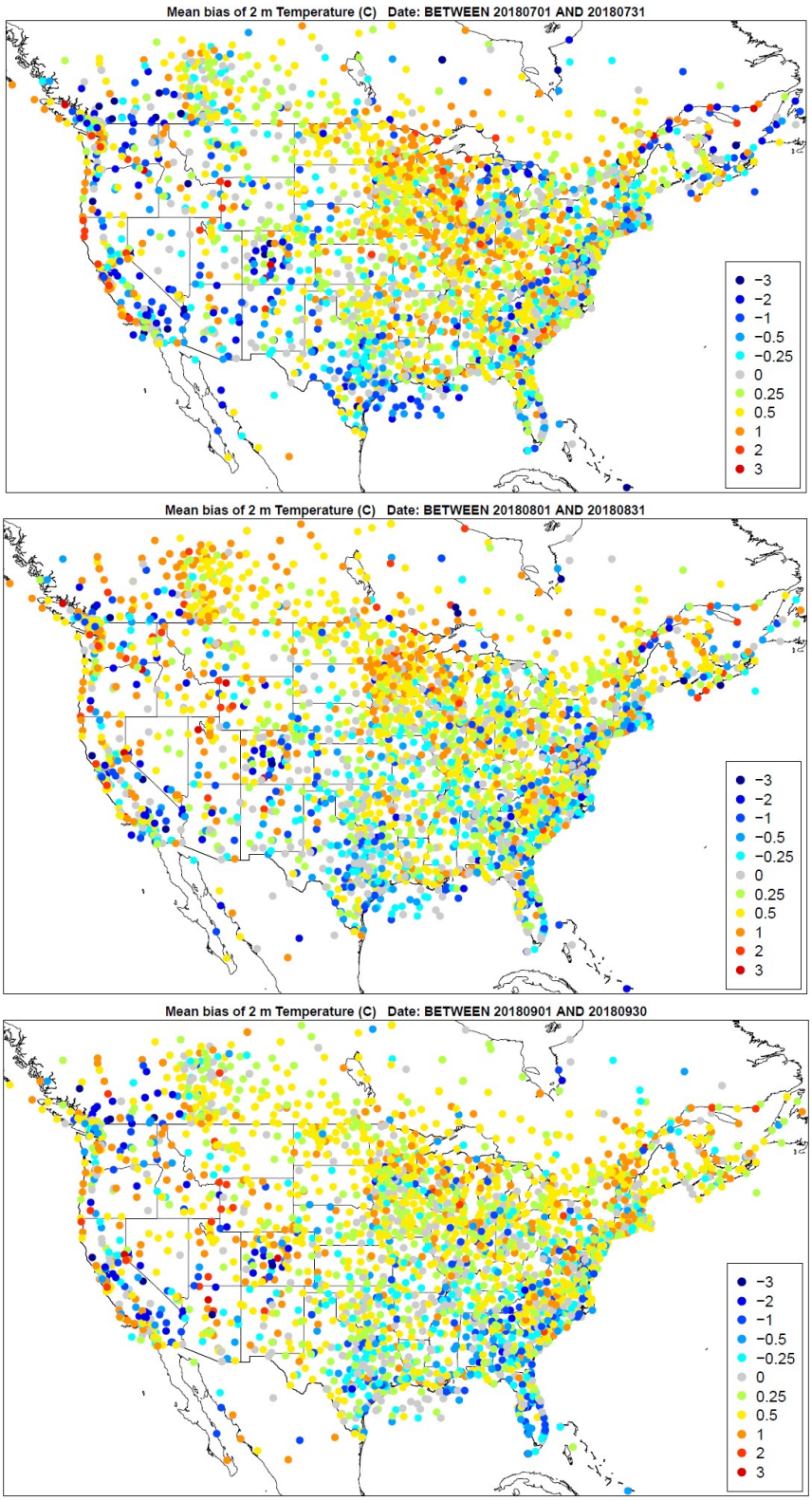

Figure 3.2.4. Spatial distribution of temperature bias (C) across all hours for the months of July, August, and September (top to bottom).

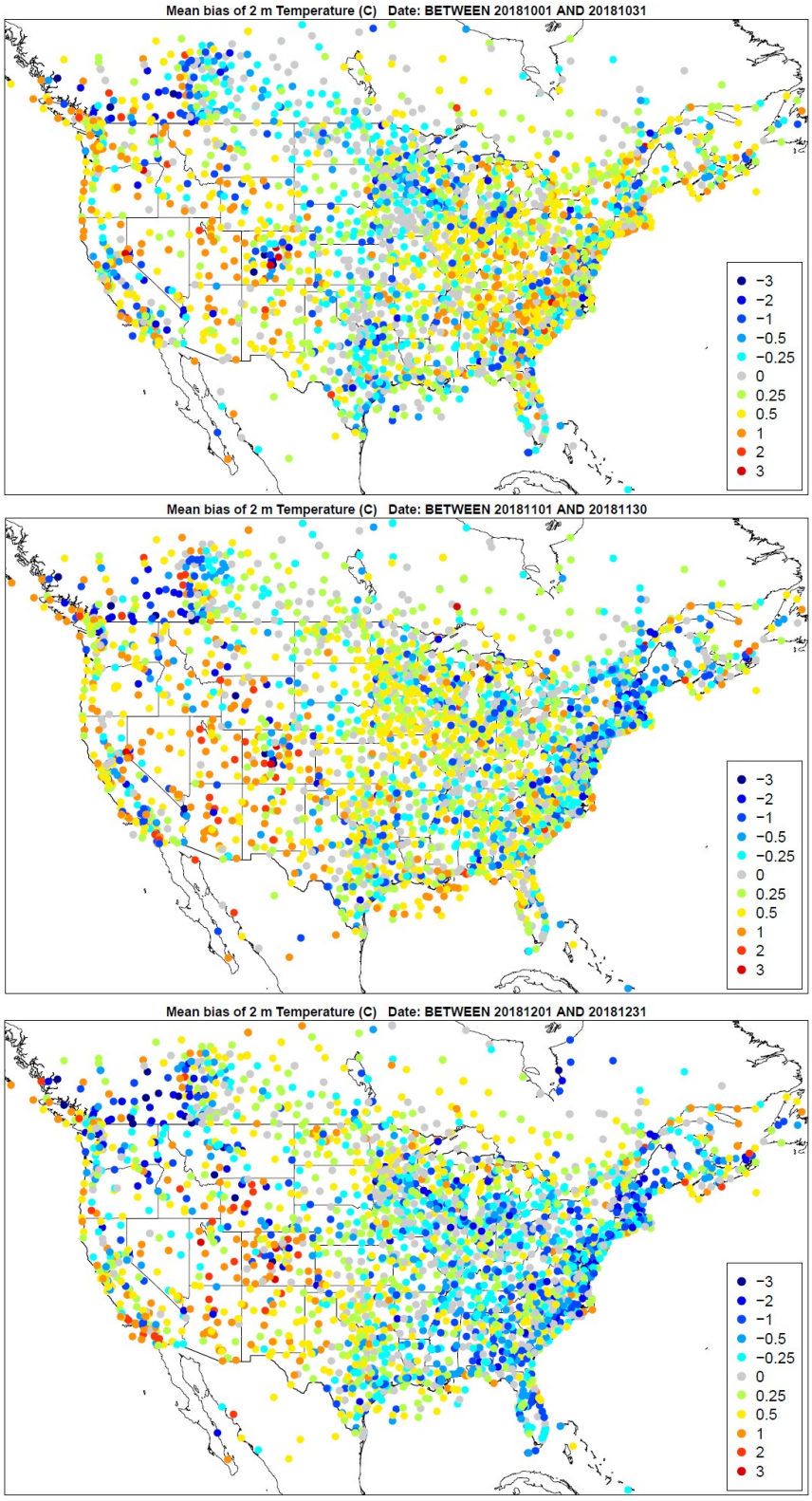

Figure 3.2.5. Spatial distribution of temperature bias (C) across all hours for the months of October, November, and December (top to bottom).

Climate Region	Season	Mean Obs	Mean Mod	MAE	MB	NMB	NME	RMSE
Northeast	Q1	273.68	273.29	1.74	-0.39	-0.14	0.64	2.34
	Q2	287.91	287.99	1.58	0.08	0.03	0.55	2.14
	Q3	295.05	295.43	1.37	0.39	0.13	0.47	1.86
	Q4	278.53	278.52	1.61	-0.01	-0.01	0.58	2.13
N. Rockies & Plains	Q1	268.76	268.97	2.08	0.21	0.08	0.77	2.77
	Q2	286.7	286.99	1.58	0.29	0.1	0.55	2.1
	Q3	292.59	293.05	1.64	0.46	0.16	0.56	2.17
	Q4	273.73	274.01	1.81	0.29	0.1	0.66	2.4
Northwest	Q1	276.89	276.89	1.57	0	0	0.57	2.1
	Q2	286.95	287.15	1.52	0.21	0.07	0.53	2.04
	Q3	292.26	292.71	1.87	0.44	0.15	0.64	2.5
	Q4	278.9	279.32	1.79	0.42	0.15	0.64	2.41
Ohio Valley	Q1	275.12	275.02	1.62	-0.09	-0.03	0.59	2.13
	Q2	291.27	291.51	1.42	0.24	0.08	0.49	1.92
	Q3	296.27	296.67	1.21	0.4	0.14	0.41	1.6
	Q4	279.56	279.74	1.42	0.18	0.06	0.51	1.88
South	Q1	283.48	283.63	1.74	0.15	0.05	0.61	2.27
	Q2	296.22	296.39	1.31	0.17	0.06	0.44	1.78
	Q3	299.94	300.13	1.25	0.18	0.06	0.42	1.68
	Q4	285.58	285.79	1.5	0.21	0.07	0.52	1.97
Southeast	Q1	284.01	284.03	1.68	0.02	0.01	0.59	2.2
	Q2	294.93	295.13	1.33	0.2	0.07	0.45	1.78
	Q3	299	299.21	1.21	0.2	0.07	0.41	1.61
	Q4	287.21	287.35	1.53	0.13	0.05	0.53	2.03
Southwest	Q1	277.43	277.83	2.19	0.39	0.14	0.79	2.87
	Q2	291.17	291.39	2.01	0.22	0.08	0.69	2.68
	Q3	295.7	296.02	2.03	0.32	0.11	0.69	2.72
	Q4	278.43	279.1	1.99	0.66	0.24	0.72	2.62
Upper Midwest	Q1	267.93	267.59	1.72	-0.34	-0.13	0.64	2.28
	Q2	286.64	286.75	1.57	0.11	0.04	0.55	2.14
	Q3	292.73	293.3	1.37	0.57	0.2	0.47	1.84
	Q4	273.67	273.79	1.43	0.12	0.04	0.52	1.97
West	Q1	283.75	283.99	1.74	0.24	0.08	0.61	2.36
	Q2	291.3	291.37	1.61	0.07	0.02	0.55	2.19
	Q3	296.68	296.86	1.84	0.19	0.06	0.62	2.52
	Q4	285.99	286.45	1.91	0.46	0.67	2.51	2.58

Table 3.2.1. Mean observed, mean modeled, mean absolute error (MAE), mean bias (MB), normalized mean bias (NMB), normalized mean error (NME), and root mean square error (RMSE) for temperature (K).

3.3 Mixing Ratio

Water mixing ratio estimates are compared to the ds472 observation network described earlier and are presented below (Figure 3.3.1). Regional analysis of statistical metrics for water vapor mixing ratio performance by quarter is shown in Table 3.3.1.

Mixing ratio is generally overpredicted across most hours of the day with a greater spread in the bias in the early morning and evening hours. Increased spread in the bias also occurs during the late Spring to early Fall when increased moisture levels across the country are noted. In general, the model error is less than a g/kg across the year and all hours of the day.

The monthly spatial distributions of the mixing ratio bias across all hours are shown in Figures 3.3.3-3.3.6. As noted in the earlier figures, a general overprediction of moisture is observed across much of the year. Some slight variations appear across regions, with a noticeable underprediction of moisture that persists across the Southeast for much of the year. Mixing ratio performance is noticeably overpredicted during the summer months across the Western US, with biases of 1-2 g/kg.

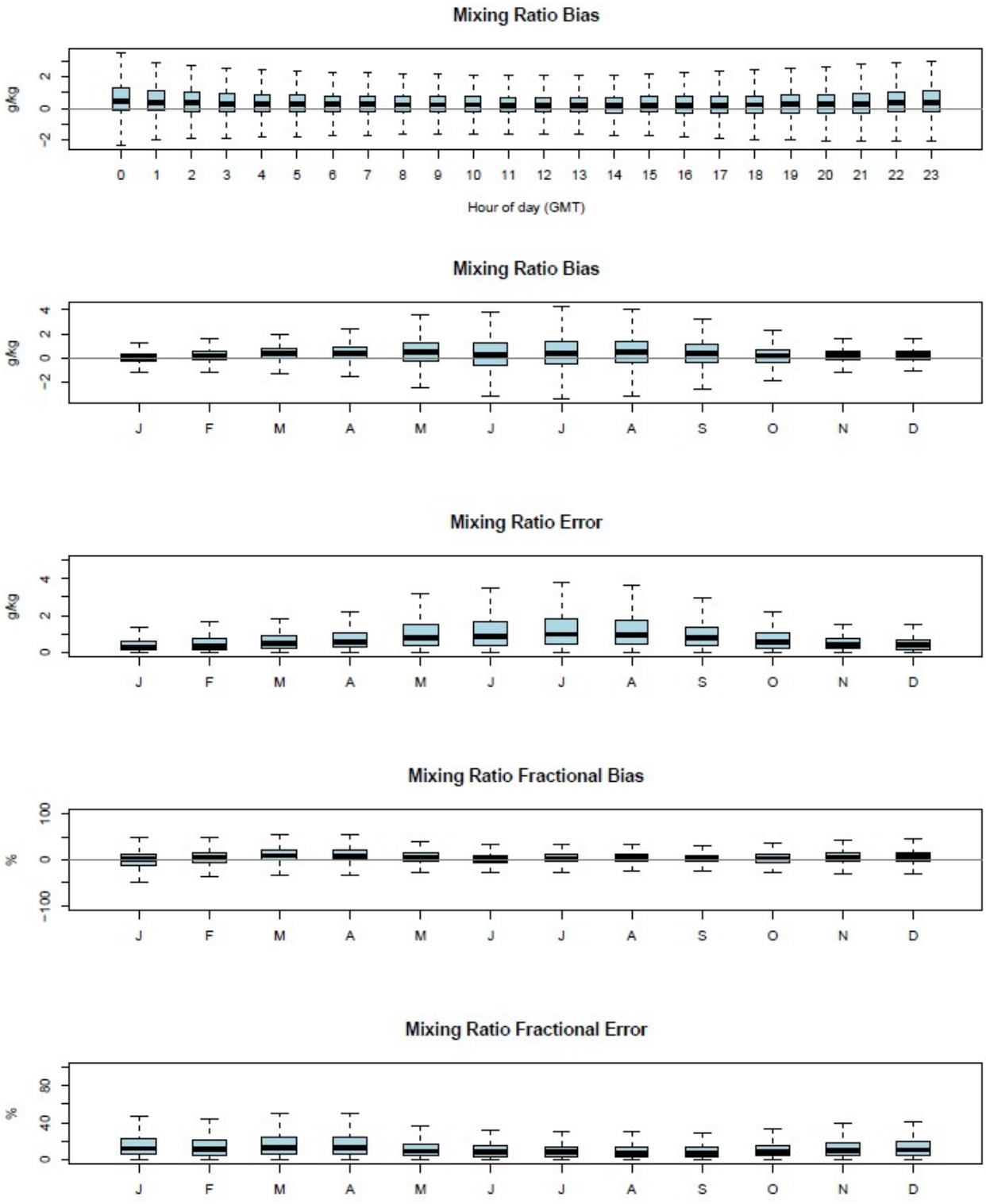

Figure 3.3.1. Distribution of hourly bias by hour and hourly bias, error, fractional bias, and fractional error for water vapor mixing ratio by month.

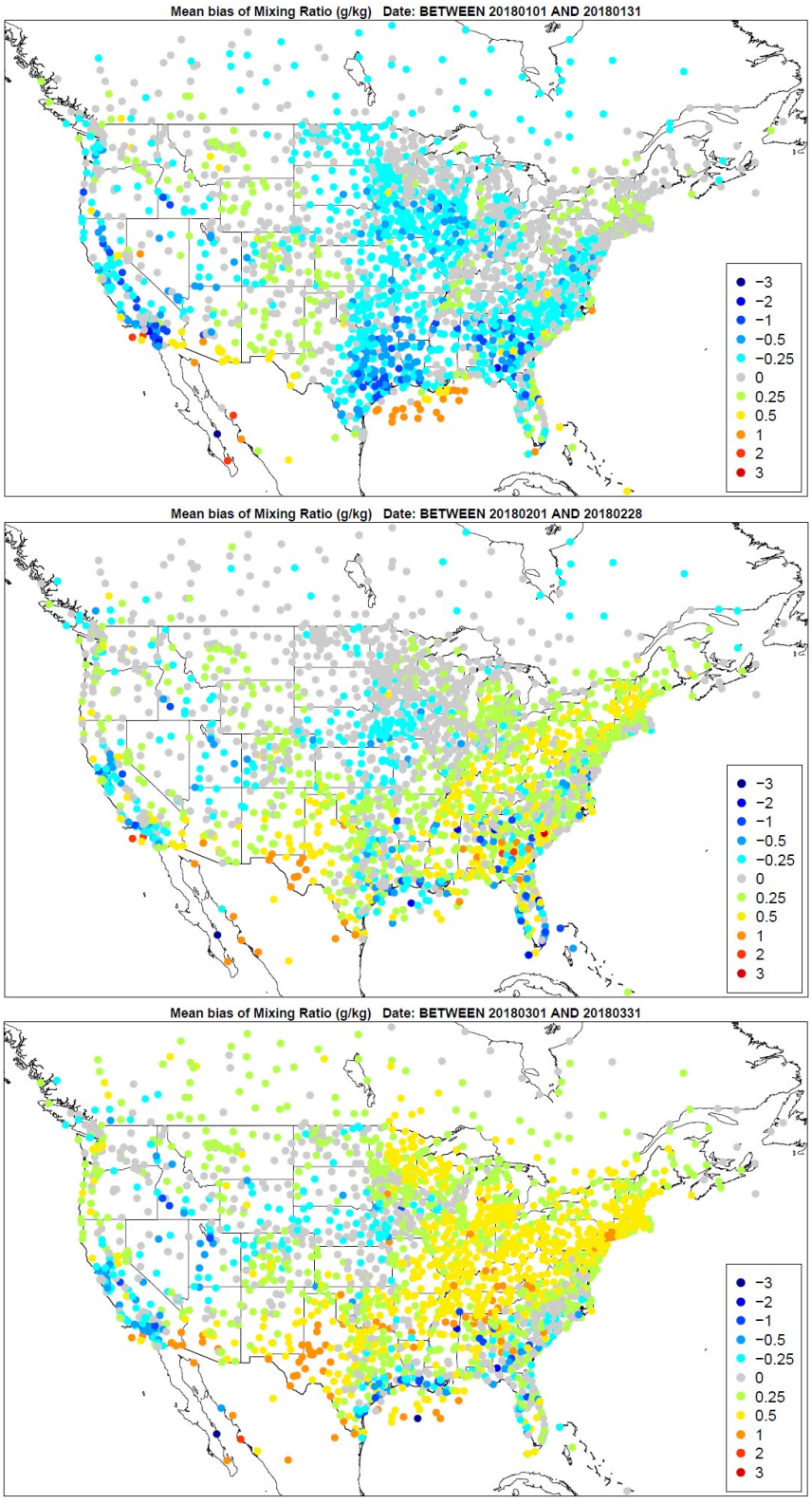

Figure 3.3.2. Spatial distribution of water vapor mixing ratio bias (g/kg) across all hours for the months of January, February, and March (top to bottom).

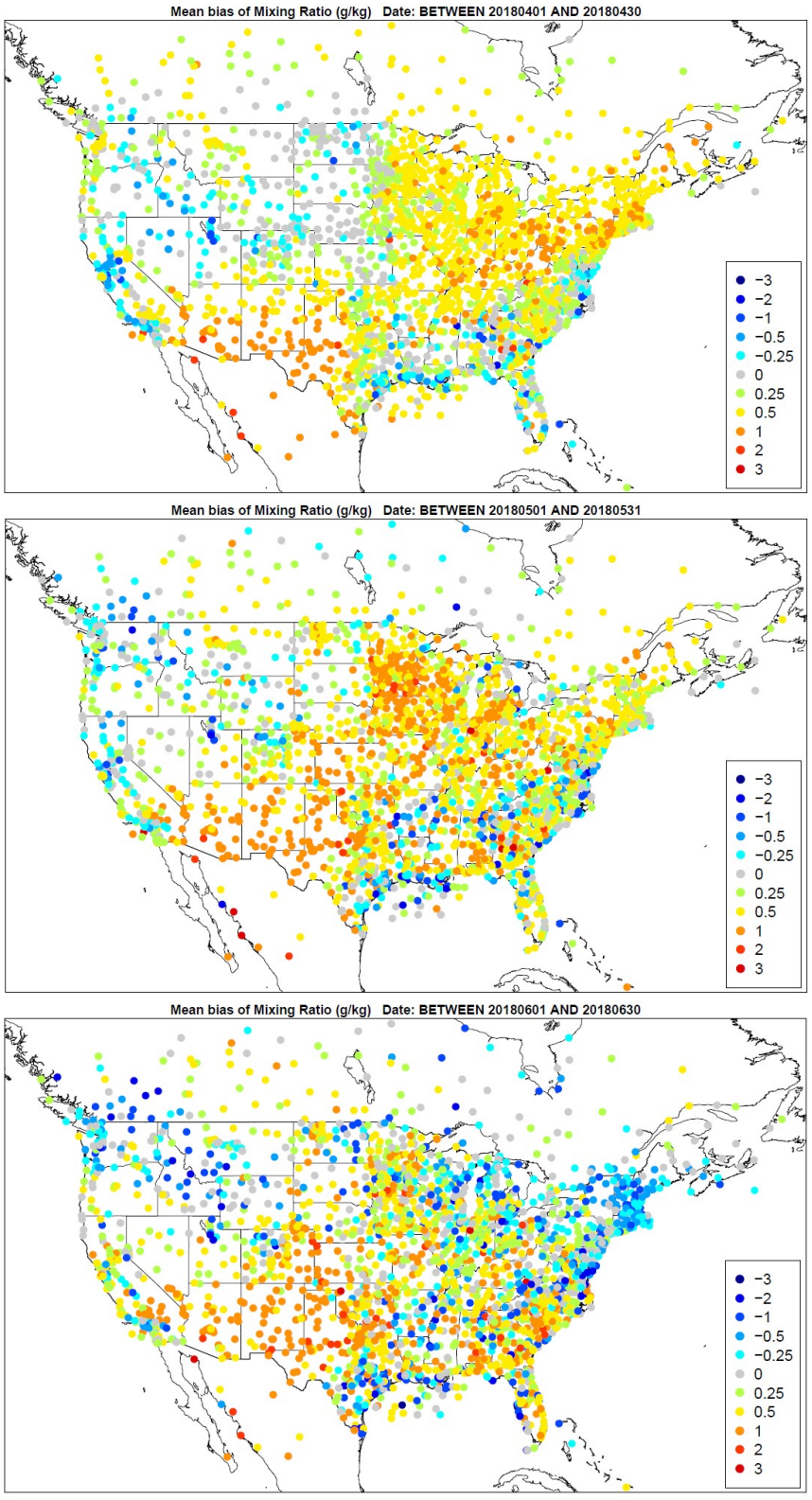

Figure 3.3.3. Spatial distribution of water vapor mixing ratio bias (g/kg) across all hours for the months of April, May, and June (top to bottom).

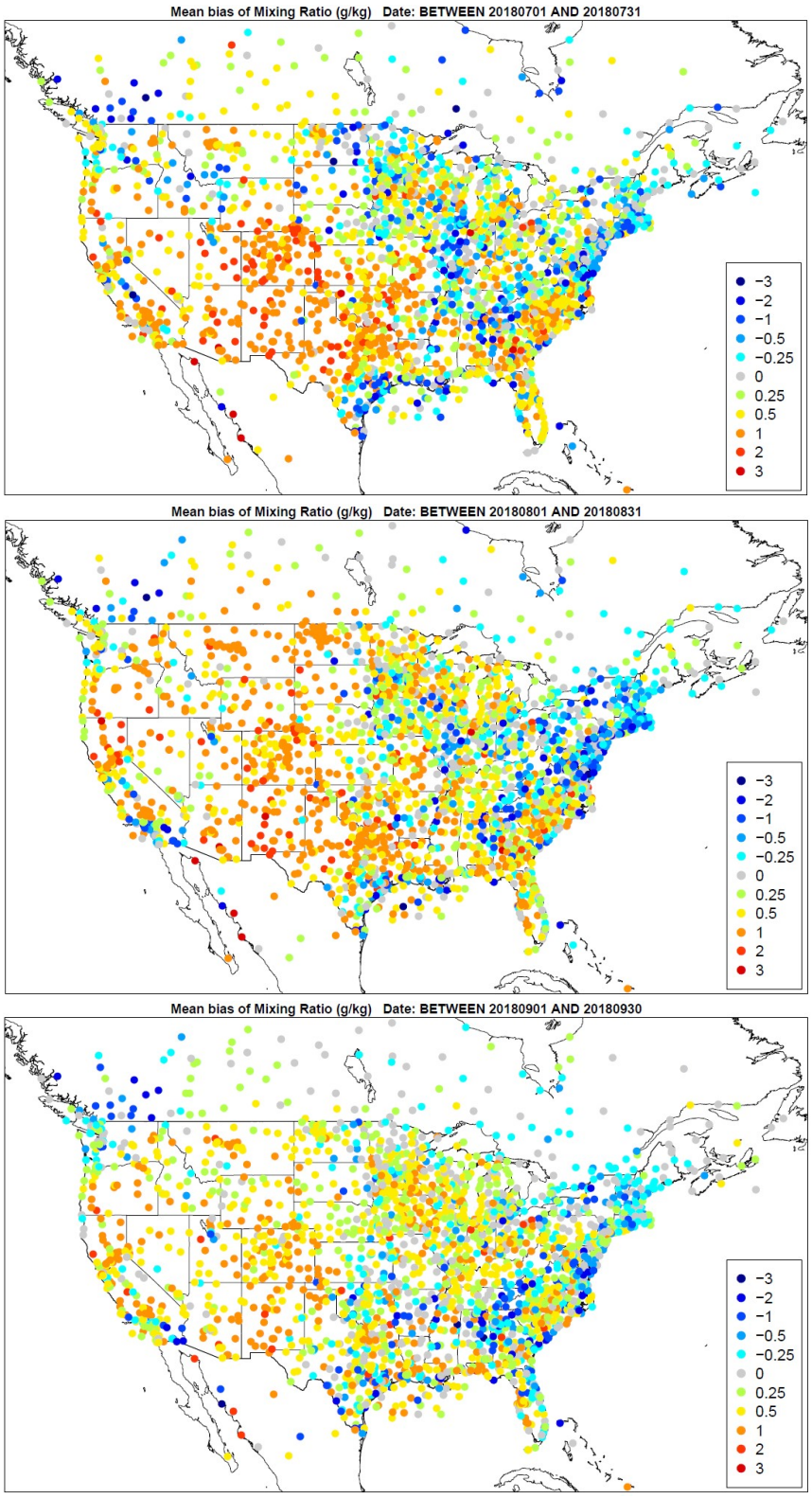

Figure 3.3.4. Spatial distribution of water vapor mixing ratio bias (g/kg) across all hours for the months of July, August, and September (top to bottom).

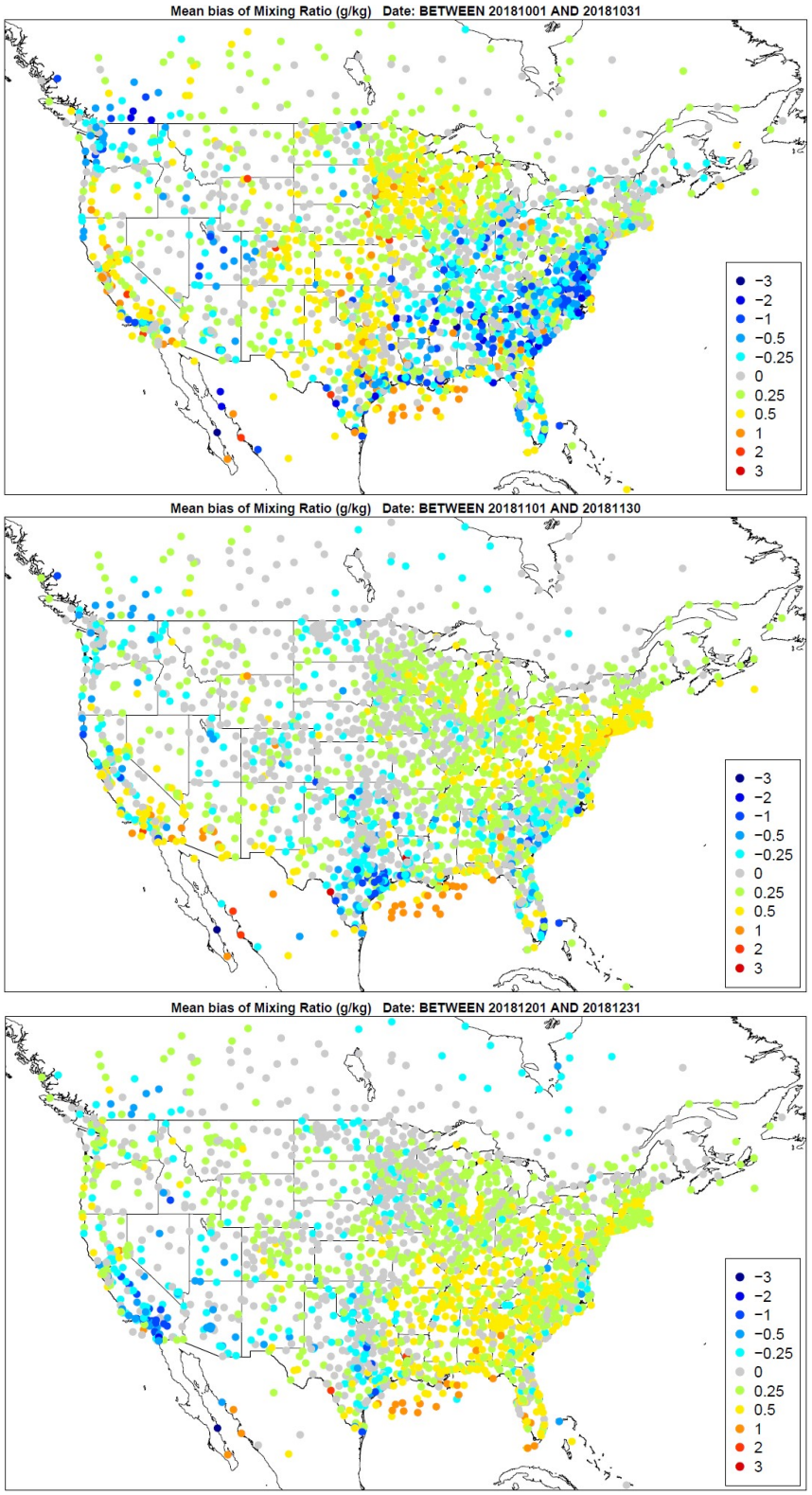

Figure 3.3.5. Spatial distribution of water vapor mixing ratio bias (g/kg) across all hours for the months of October, November, and December (top to bottom).

Climate Region	Season	Mean Obs	Mean Mod	MAE	MB	NMB	NME	RMSE
Northeast	Q1	3.22	3.62	0.57	0.4	12.56	17.66	0.79
	Q2	7.99	8.42	0.94	0.44	5.47	11.82	1.25
	Q3	13.42	13.44	0.98	0.02	0.11	7.3	1.31
	Q4	4.96	5.31	0.63	0.36	7.24	12.7	0.84
N. Rockies & Plains	Q1	2.46	2.56	0.38	0.1	4.06	15.57	0.53
	Q2	7.44	7.76	0.92	0.32	4.34	12.4	1.33
	Q3	9.77	10.38	1.2	0.61	6.24	12.3	1.62
	Q4	3.34	3.58	0.43	0.24	7.04	12.96	0.61
Northwest	Q1	4.18	4.32	0.48	0.14	3.38	11.4	0.67
	Q2	6.46	6.55	0.71	0.09	1.41	11	0.98
	Q3	7.15	7.73	1.03	0.58	8.17	14.37	1.42
	Q4	4.78	4.9	0.57	0.12	2.41	11.84	0.76
Ohio Valley	Q1	3.75	4.05	0.59	0.31	8.25	15.78	0.88
	Q2	10.35	10.97	1.1	0.62	6.01	10.6	1.47
	Q3	14.25	14.59	1.09	0.34	2.41	7.67	1.48
	Q4	5.36	5.64	0.6	0.28	5.23	11.1	0.83
South	Q1	6.17	6.38	0.72	0.21	3.45	11.69	1.05
	Q2	12.44	12.98	1.16	0.54	4.31	9.29	1.58
	Q3	15.8	16.41	1.31	0.62	3.9	8.32	1.73
	Q4	7.72	7.96	0.75	0.24	3.1	9.71	1.08
Southeast	Q1	6.59	6.75	0.73	0.16	2.42	11.05	1.05
	Q2	12.73	13.16	1.12	0.42	3.31	8.77	1.52
	Q3	16.99	17.37	1.25	0.38	2.23	7.33	1.64
	Q4	8.84	9.03	0.85	0.19	2.18	9.64	1.16
Southwest	Q1	2.8	3.05	0.57	0.24	8.71	20.52	0.8
	Q2	4.47	5.19	1.14	0.72	16.02	25.45	1.51
	Q3	8.48	9.64	1.57	1.16	13.66	18.5	2.01
	Q4	4.01	4.21	0.61	0.2	5.12	15.21	0.88
Upper Midwest	Q1	2.25	2.42	0.38	0.17	7.36	16.91	0.61
	Q2	7.78	8.39	1.04	0.61	7.9	13.36	1.46
	Q3	11.7	12.13	1.02	0.43	3.64	8.71	1.38
	Q4	3.63	3.96	0.47	0.33	9.07	12.87	0.68
West	Q1	5.08	5.07	0.73	-0.01	-0.19	14.35	1.05
	Q2	6.77	7.06	0.87	0.29	4.26	12.82	1.22
	Q3	8.76	9.4	1.26	0.64	7.34	14.34	1.7
	Q4	5.64	5.85	0.88	0.21	3.81	15.52	1.23

Table 3.3.1. Mean observed, mean modeled, mean absolute error (MAE), mean bias (MB), normalized mean bias (NMB), normalized mean error (NME), and root mean square error (RMSE) for water vapor mixing ratio (g/kg).

3.4 Precipitation

Monthly total rainfall is plotted for each grid cell to assess how well the model captures the spatial variability and magnitude of convective and non-convective rainfall. As described earlier, the PRISM estimations for rainfall are only within the continental United States. With lightning assimilation mentioned earlier, the model will either trigger (suppress) convection when lightning is observed (not observed). This assimilation is particularly useful in constraining the model's convection scheme that at times has been observed to be inaccurately active. WRF rainfall estimates by month are shown for all grid cells in the domain. Monthly total estimates are shown in Figures 3.4.1 through 3.4.12.

Overall, the model captures the general spatial patterns and magnitude of the precipitation across the US throughout the year. Precipitation is generally underpredicted across the southern US during February and October through December. There is a general overprediction that is noted across the western US, particularly in areas of complex terrain (e.g., northern CA, the Rockies, etc.), especially during the Summer months. It should also be noted there is a slight overprediction of precipitation during March and April in the Northeast.

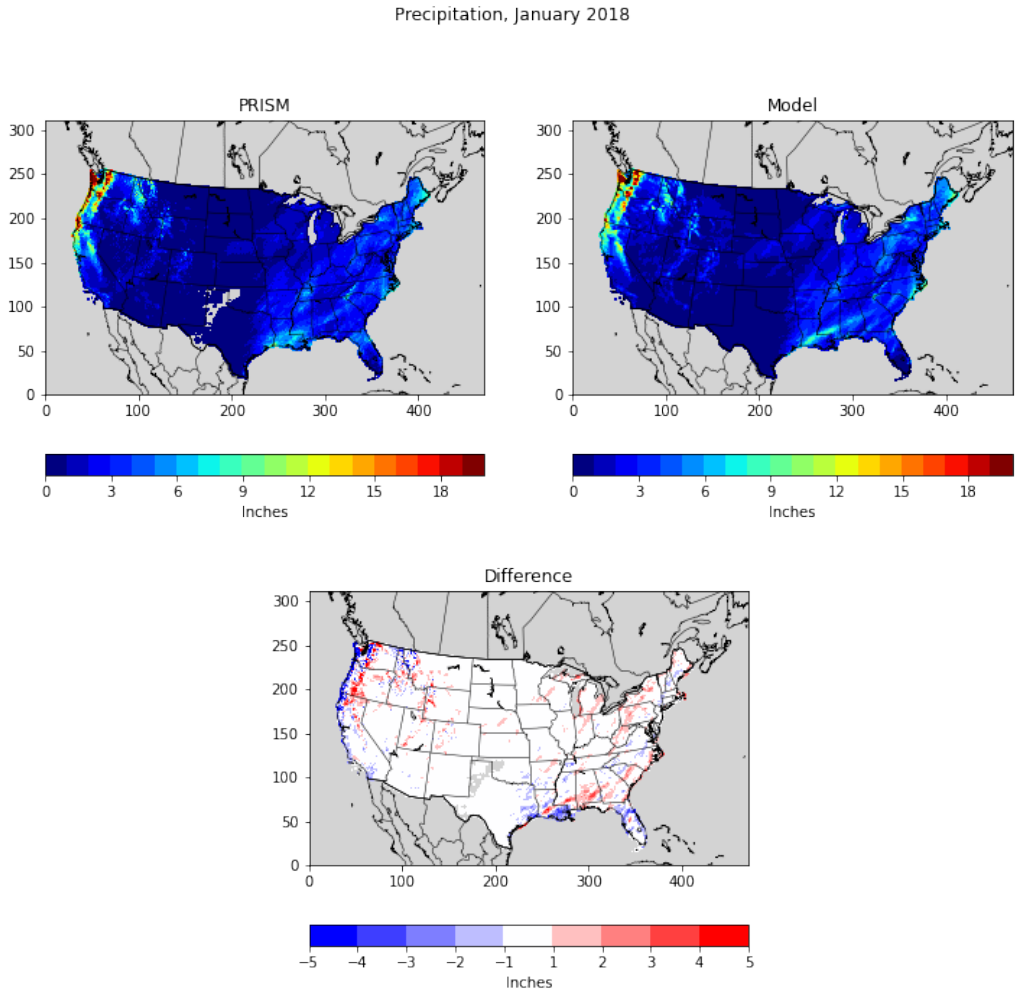

Figure 3.4.1. PRISM analysis (top left) and WRF (top right) estimated monthly total rainfall (in) and the difference (bottom) for January.

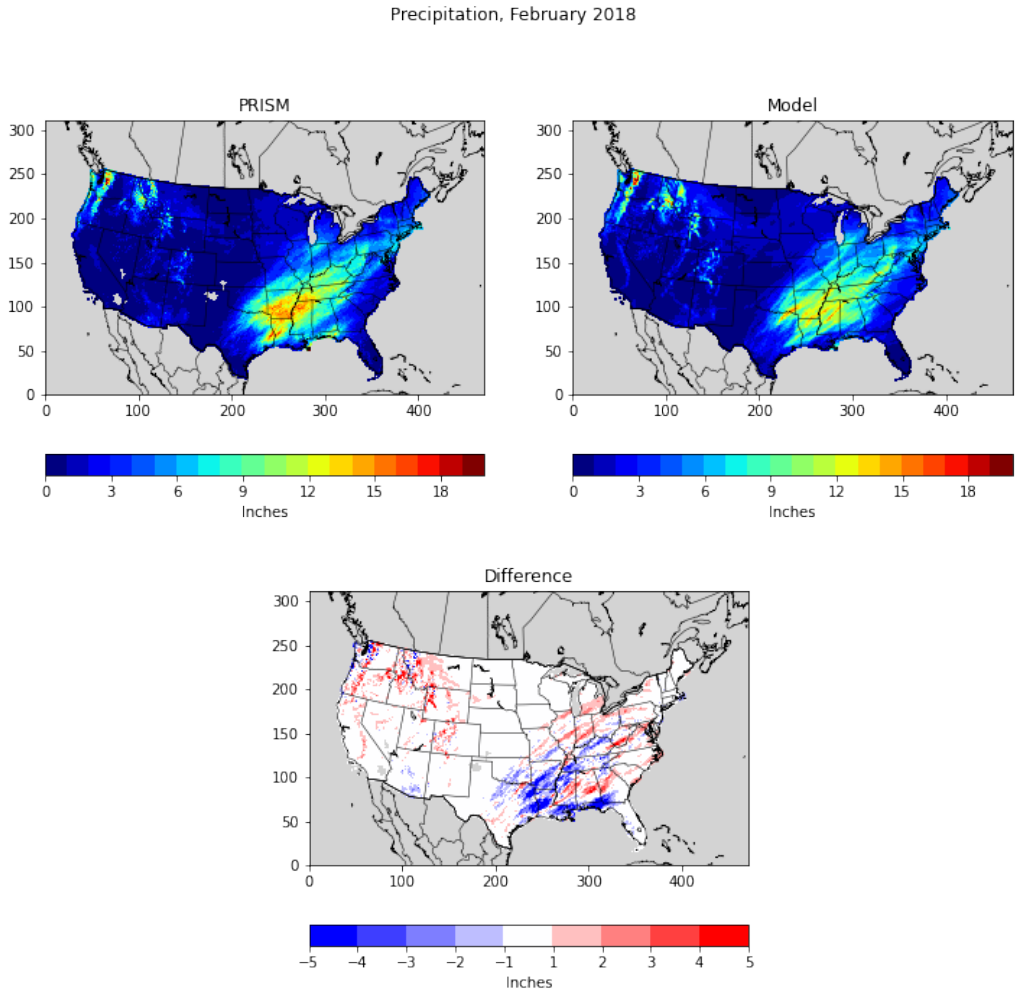

3.4.2. PRISM analysis (top left) and WRF (top right) estimated monthly total rainfall (in) and the difference (bottom) for February.

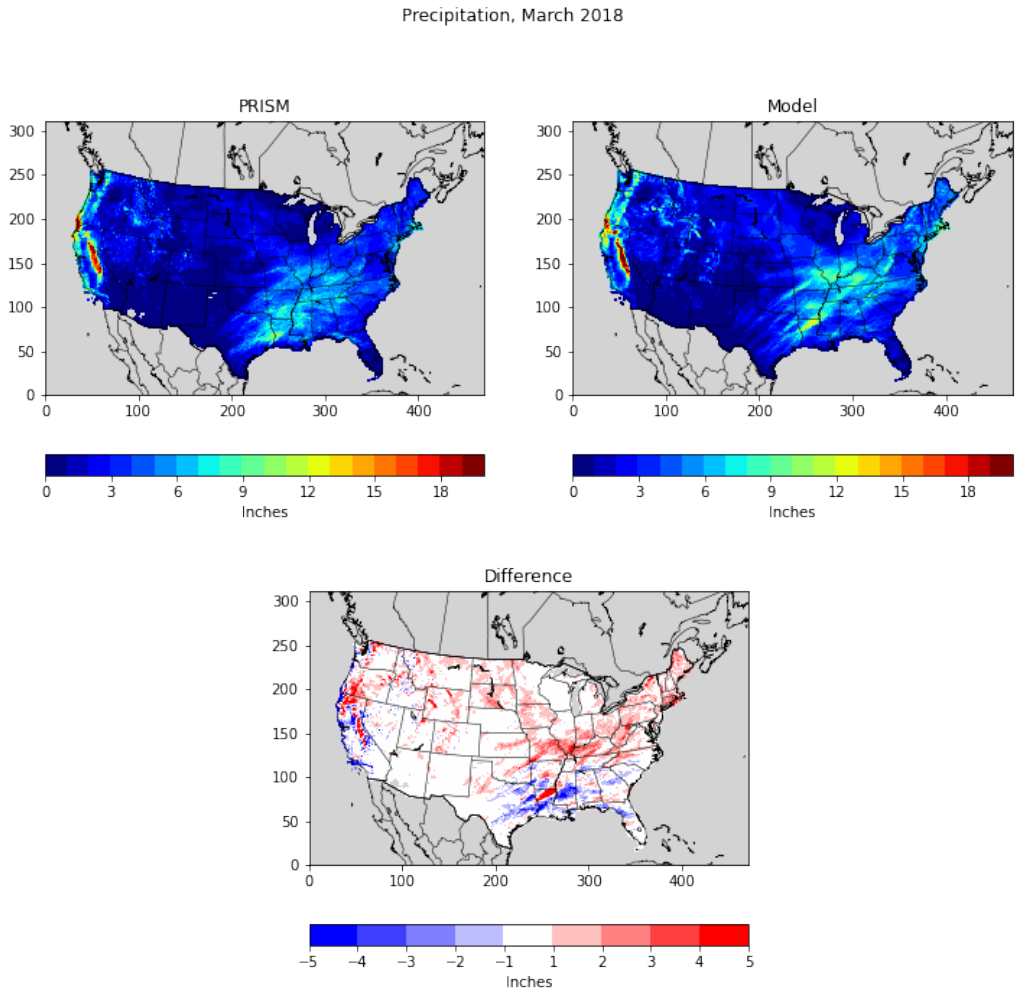

Figure 3.4.3. PRISM analysis (top left) and WRF (top right) estimated monthly total rainfall (in) and the difference (bottom) for March.

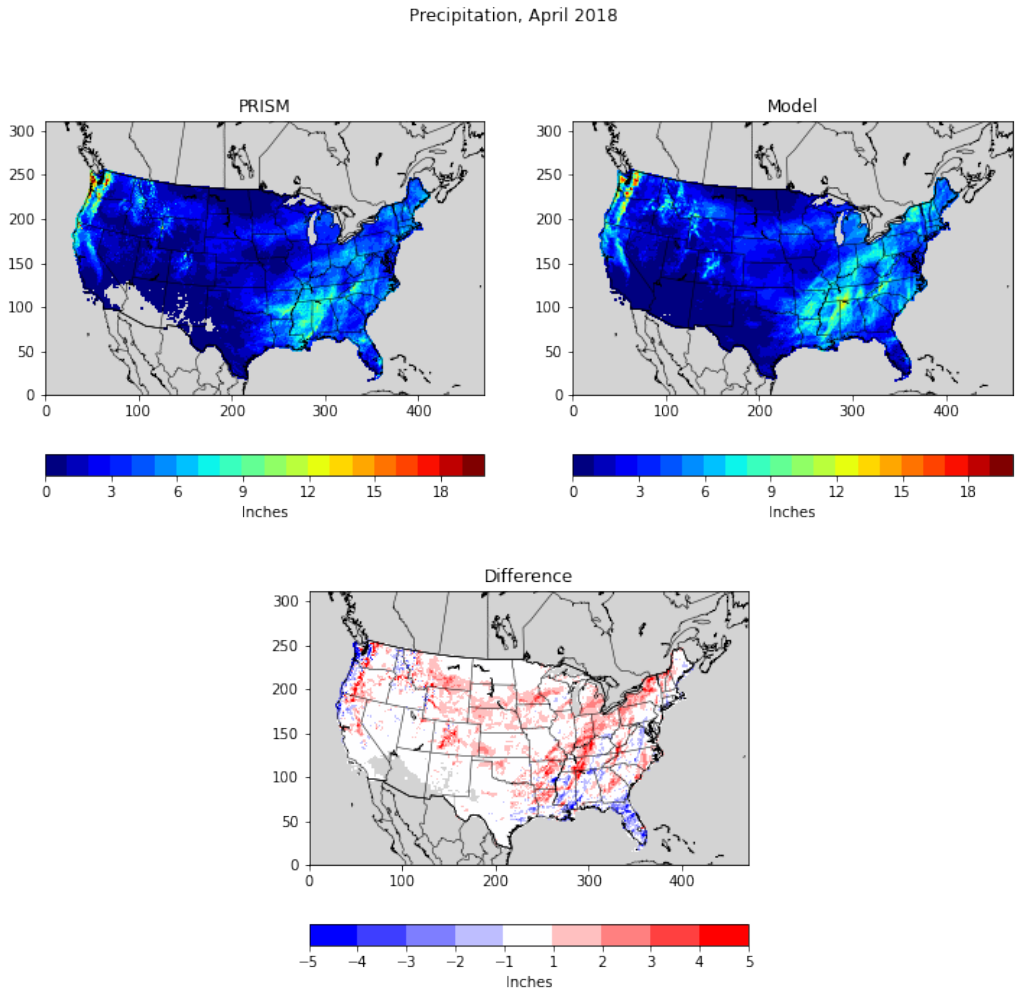

Figure 3.4.4. PRISM analysis (top left) and WRF (top right) estimated monthly total rainfall (in) and the difference (bottom) for April.

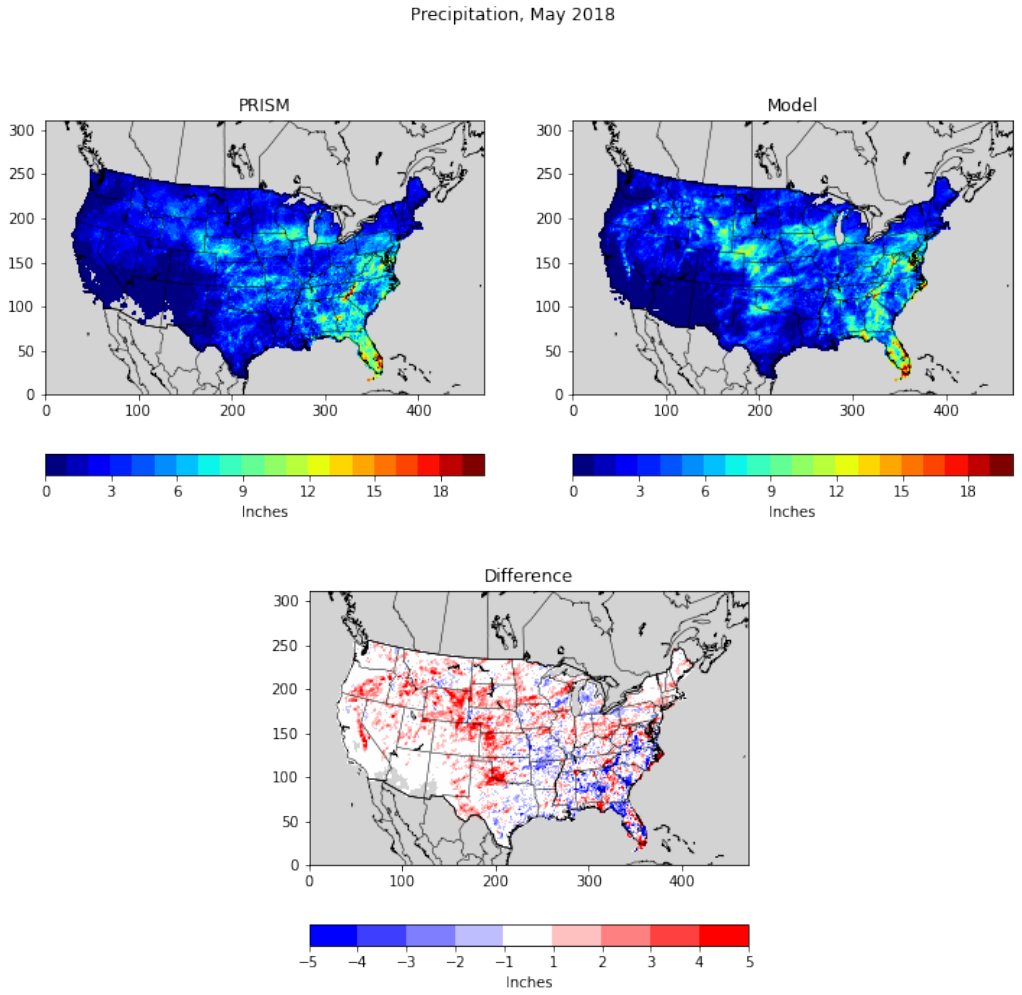

Figure 3.4.5. PRISM analysis (top left) and WRF (top right) estimated monthly total rainfall (in) and the difference (bottom) for May.

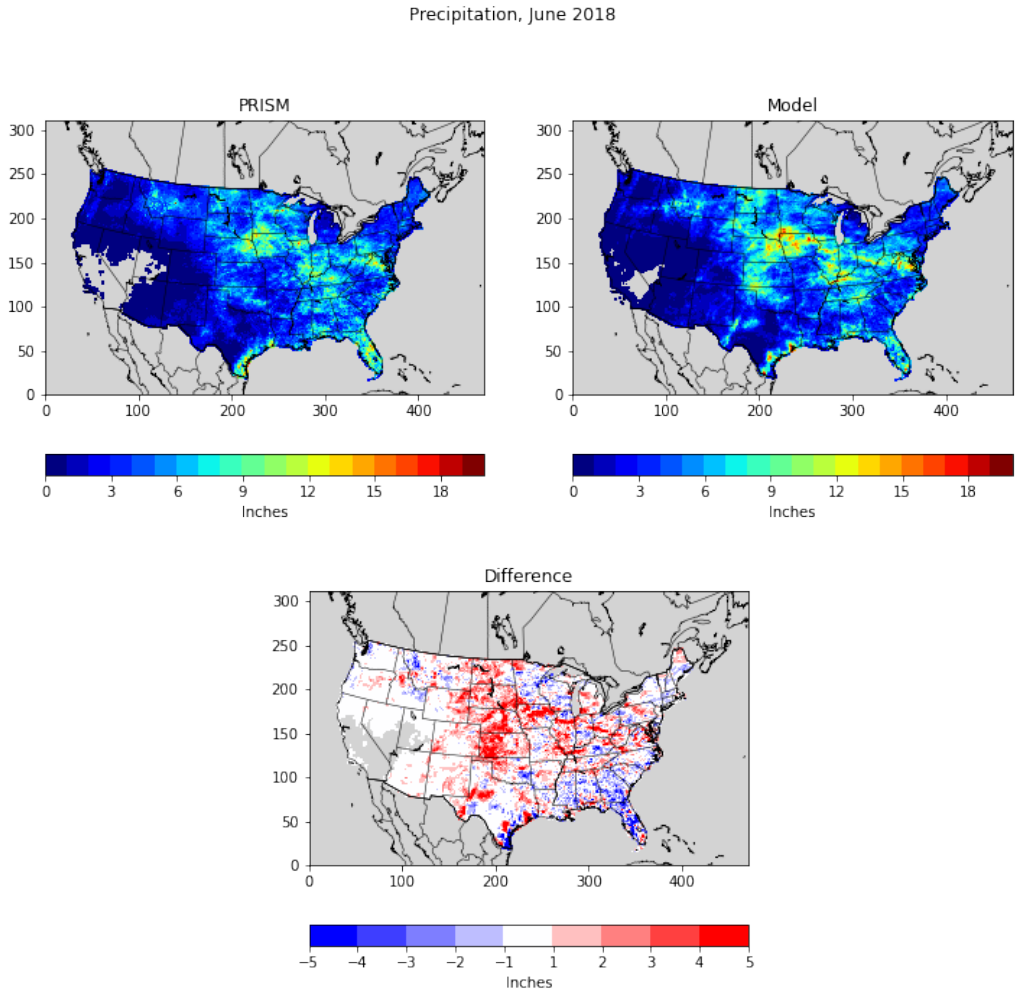

Figure 3.4.6. PRISM analysis (top left) and WRF (top right) estimated monthly total rainfall (in) and the difference (bottom) for June.

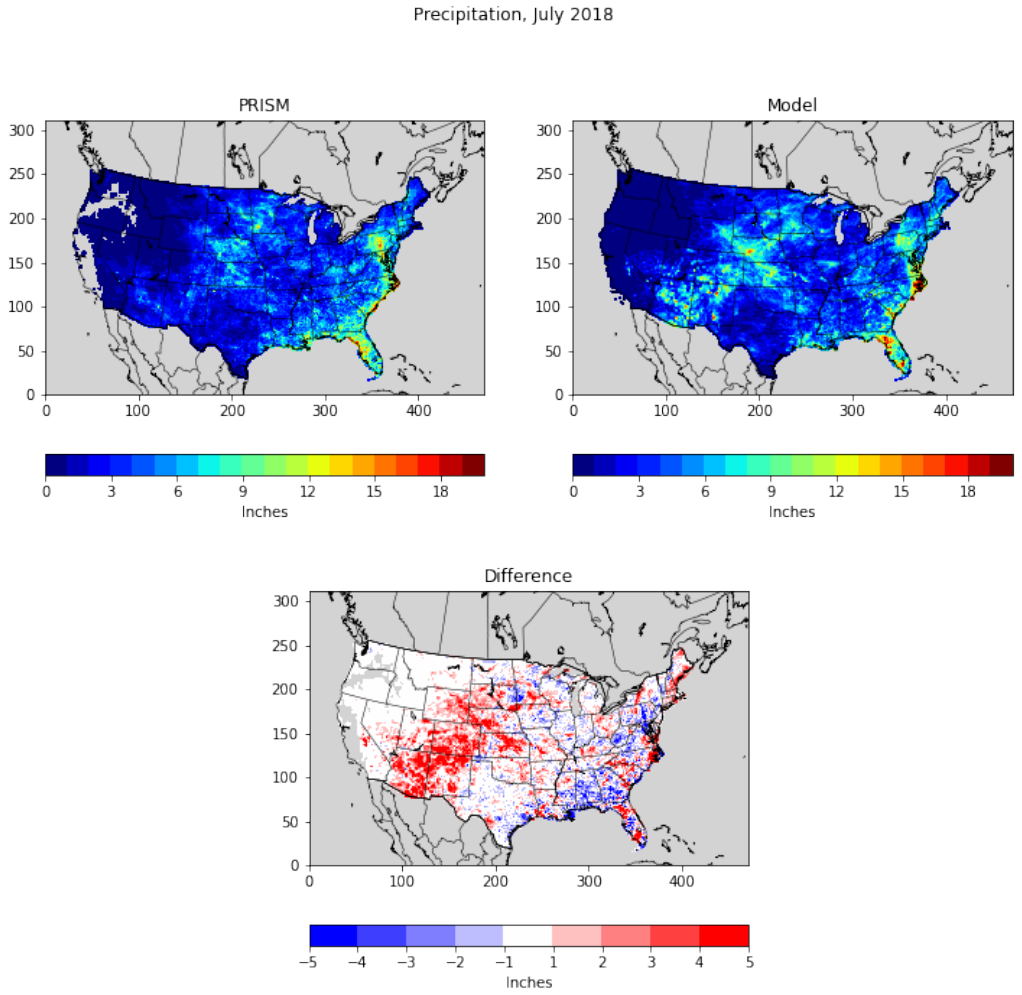

Figure 3.4.7. PRISM analysis (top left) and WRF (top right) estimated monthly total rainfall (in) and the difference (bottom) for July.

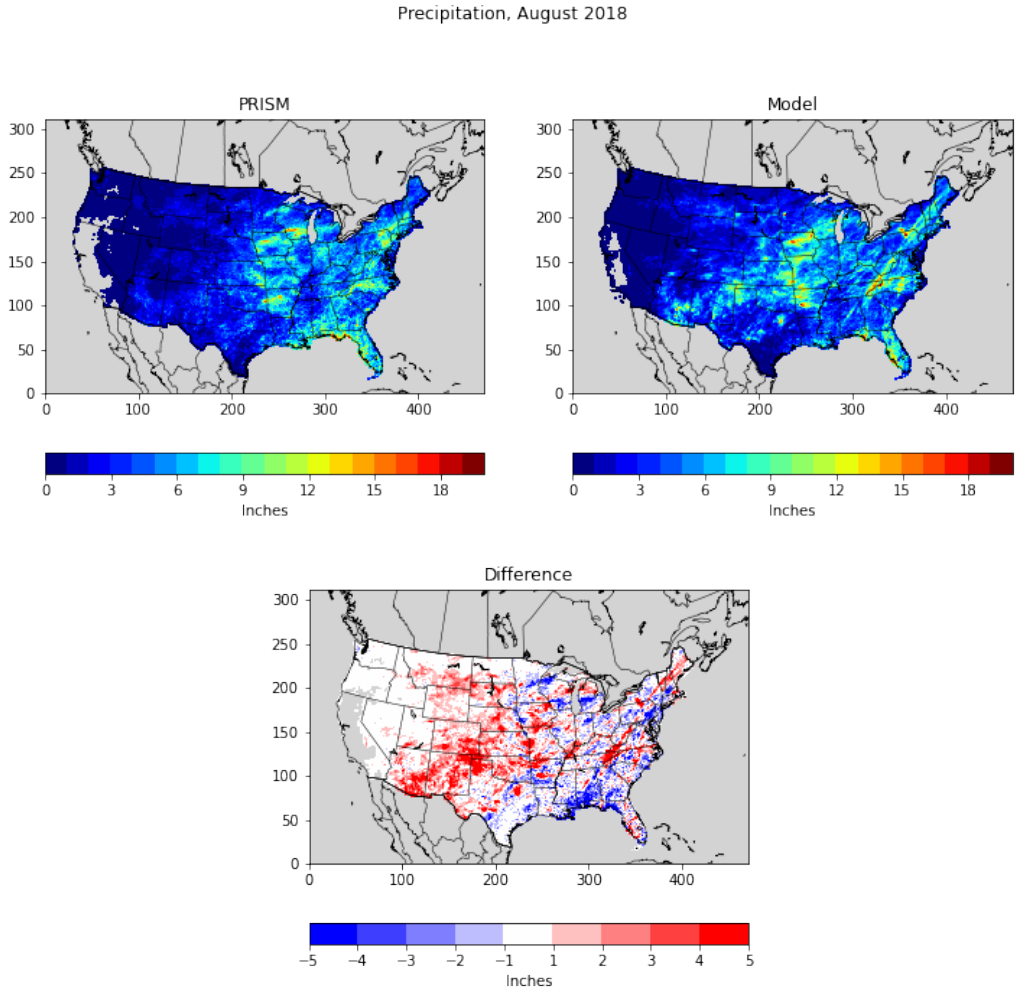

Figure 3.4.8. PRISM analysis (top left) and WRF (top right) estimated monthly total rainfall (in) and the difference (bottom) for August.

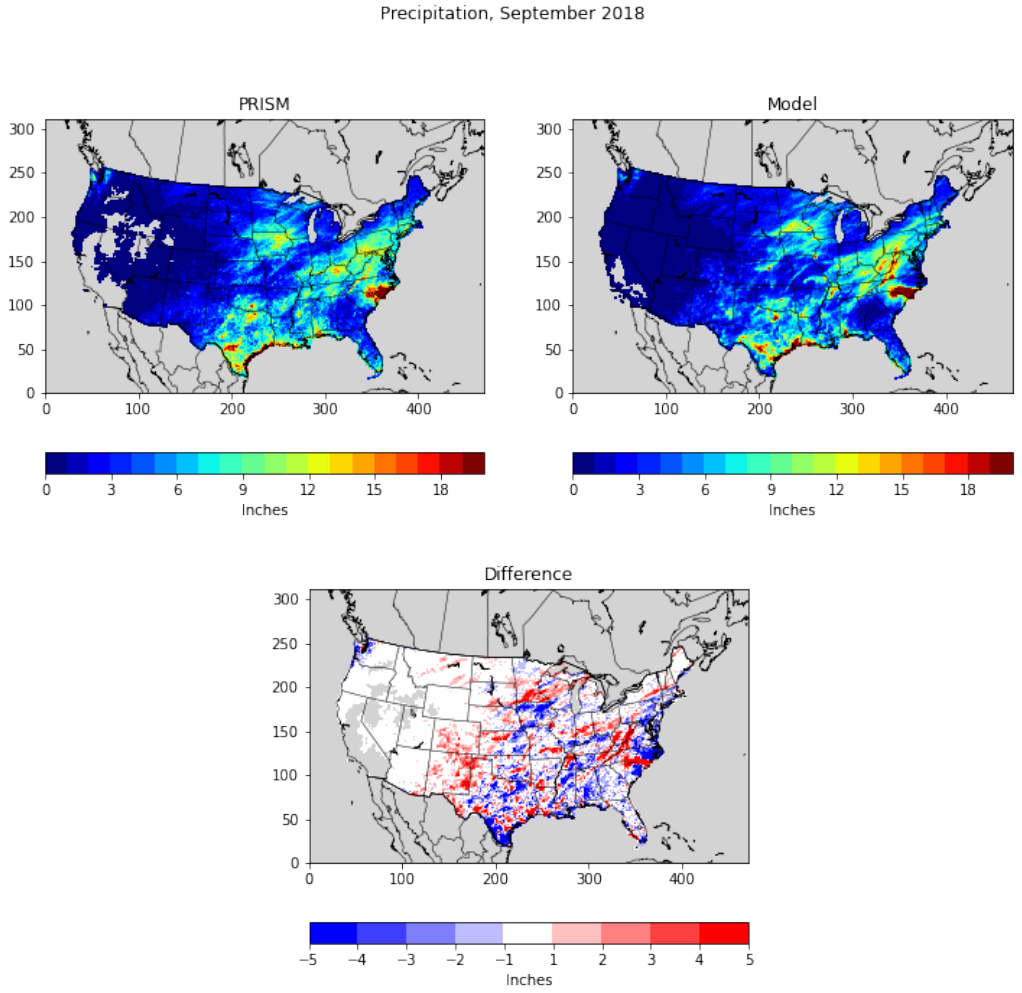

Figure 3.4.9. PRISM analysis (top left) and WRF (top right) estimated monthly total rainfall (in) and the difference (bottom) for September.

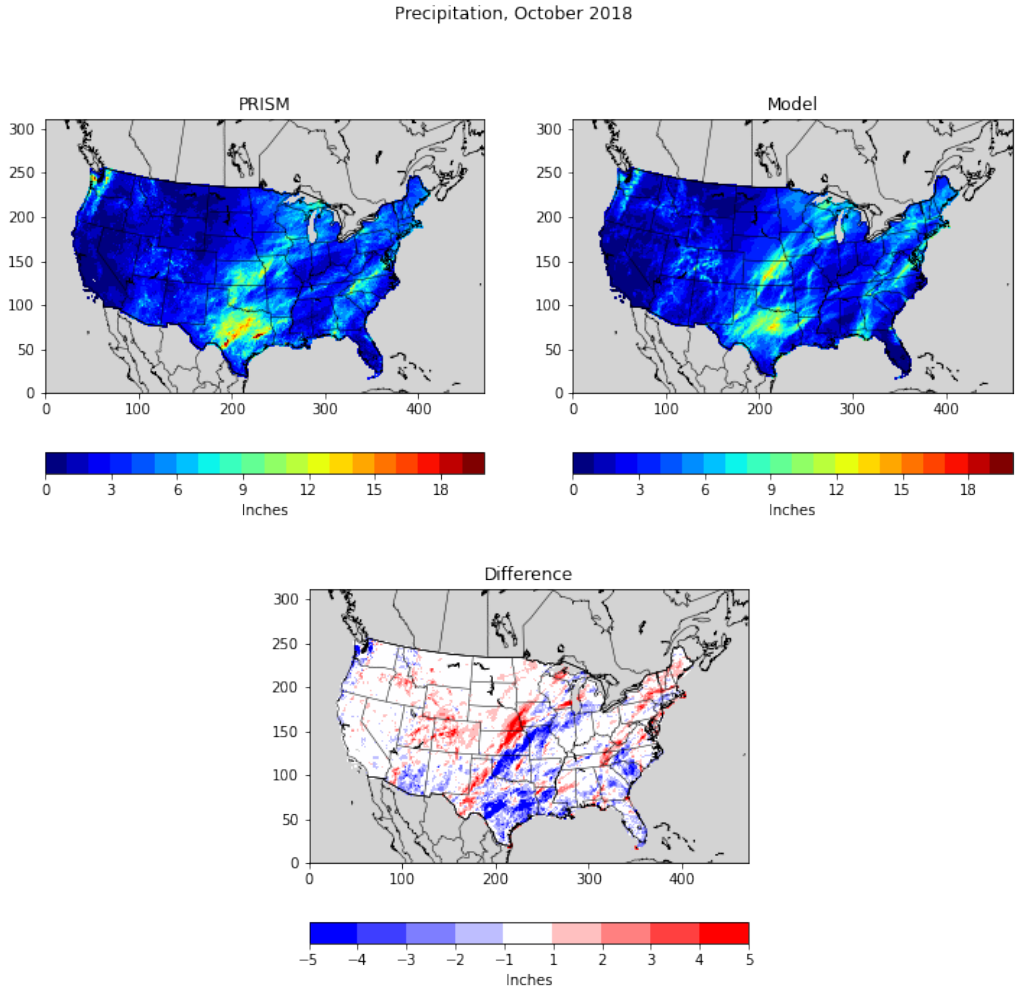

Figure 3.4.10. PRISM analysis (top left) and WRF (top right) estimated monthly total rainfall (in) and the difference (bottom) for October.

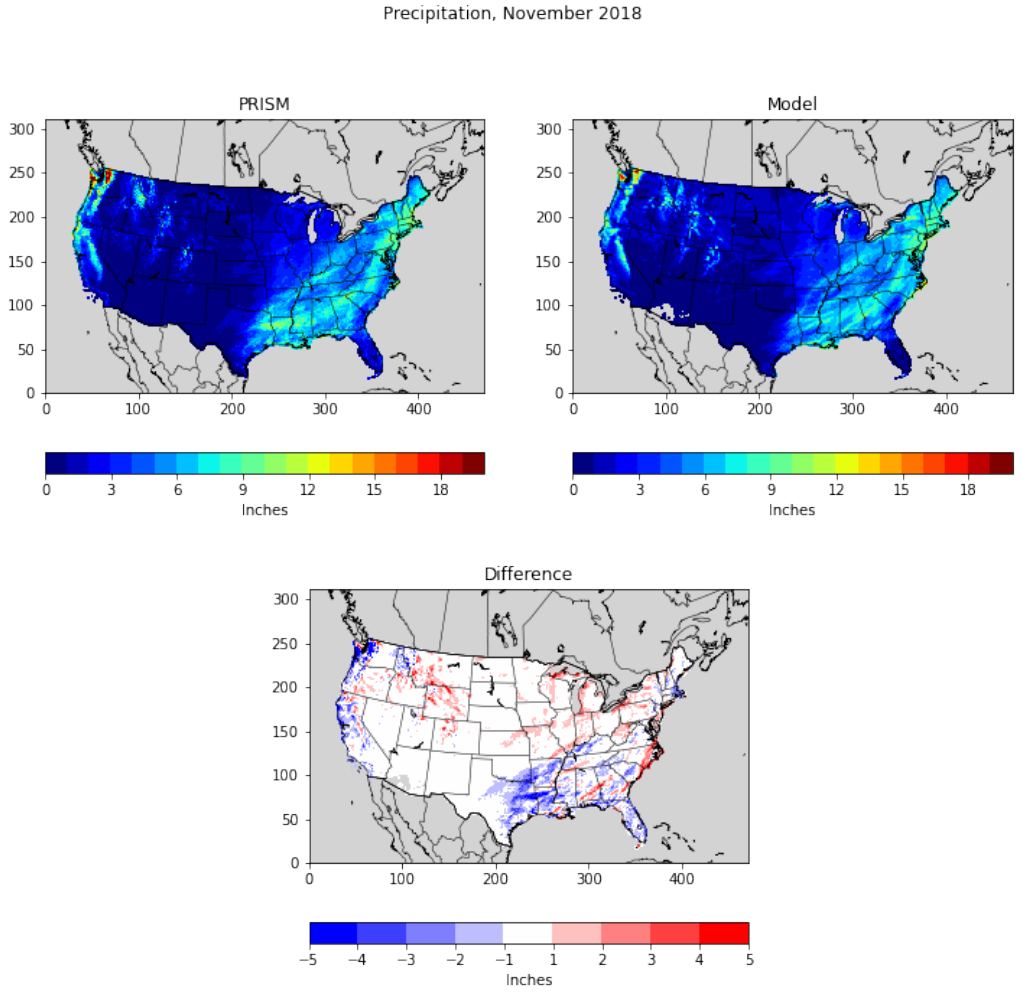

Figure 3.4.11. PRISM analysis (top left) and WRF (top right) estimated monthly total rainfall (in) and the difference (bottom) for November.

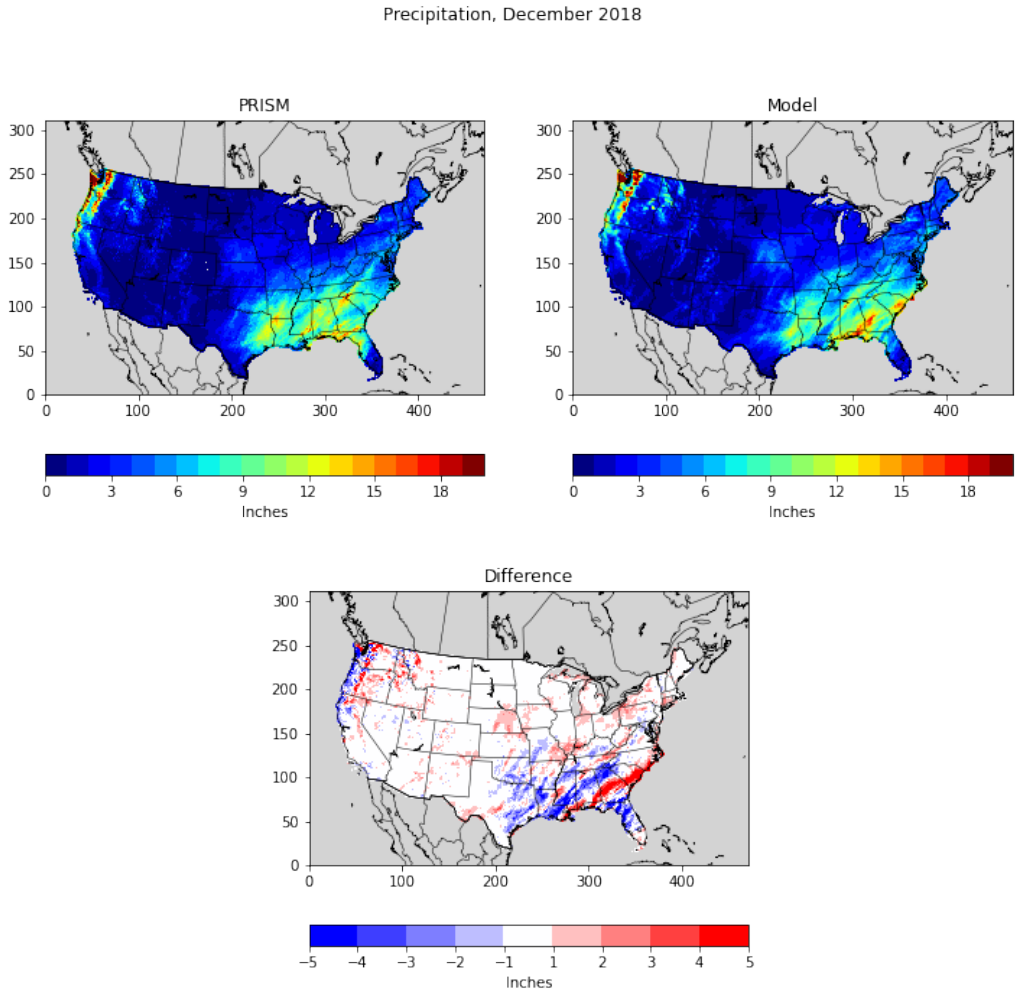

Figure 3.4.12. PRISM analysis (top left) and WRF (top right) estimated monthly total rainfall (in) and the difference (bottom) for December.

3.5 Solar Radiation

Photosynthetically activated radiation (PAR) is a fraction of shortwave downward radiation and is an important input for the biogenic emissions model for estimating isoprene (Carlton and Baker, 2011). Isoprene emissions are important for regional ozone chemistry and play a role in secondary organic aerosol formation. Radiation performance evaluation also gives an indirect assessment of how well the model captures cloud formation during daylight hours.

Shortwave downward radiation estimates are compared to surface-based measurements and shown below (Figure 3.5.1).

In general, WRF slightly overpredicts shortwave radiation across all months of the year, showing a greater spread in the overprediction during the late Spring to early Fall months. Overall, the median bias in WRF for all months of the year is roughly 10-30 W/m^2.

More variability is noted on an hourly basis as WRF overpredicts shortwave radiation across all daytime hours. The median bias during the hours of most downward shortwave radiation is less than 20-30 W/m^2. A greater spread in the overprediction is noted during the afternoon to early evening hours when the sun is highest in the sky. The model's inability to accurately simulate subgrid clouds at a 12km resolution is likely the cause of these errors.

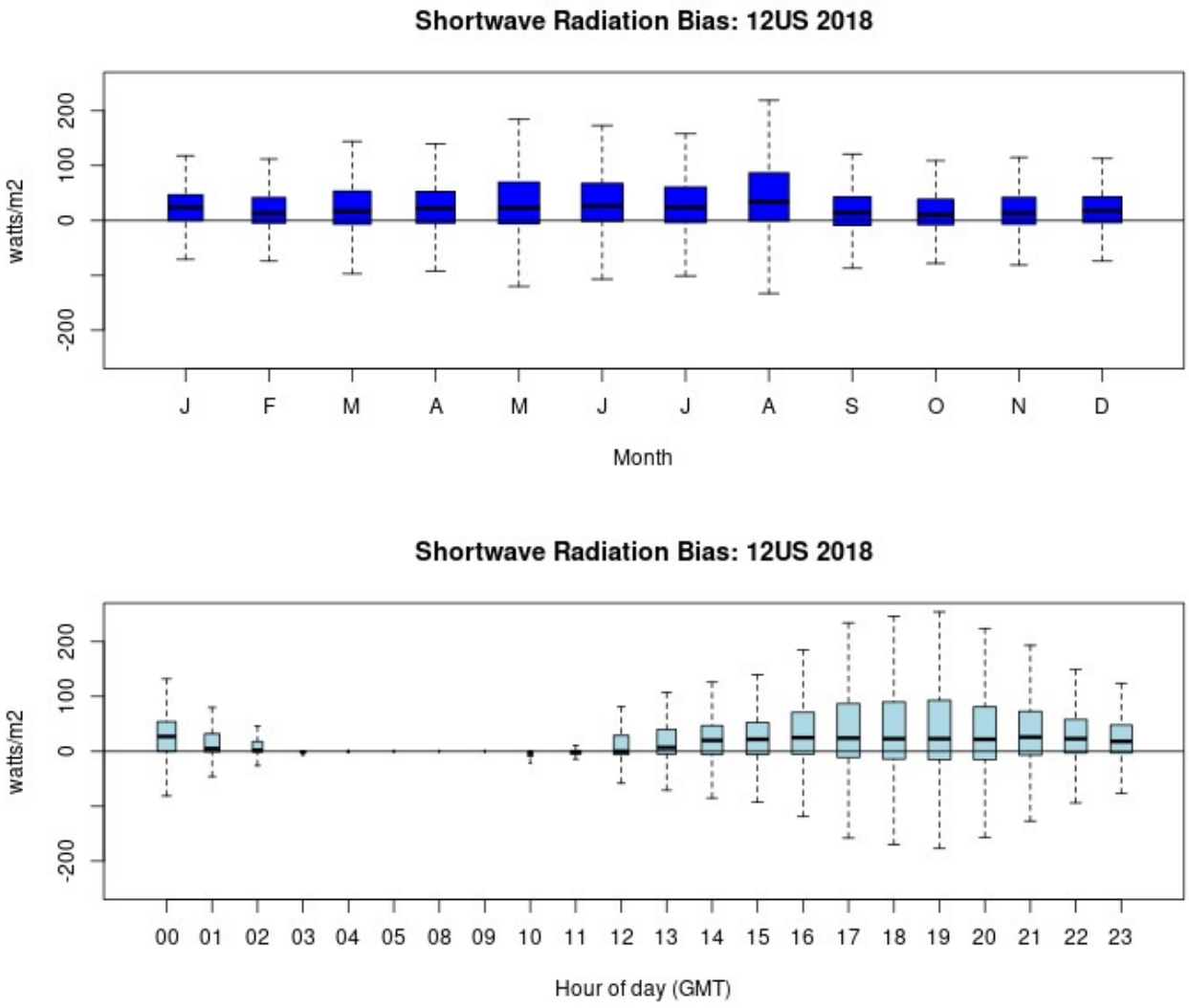

Figure 3.5.1. Distribution of hourly bias for shortwave radiation (W/m^2) by month (top) and by

4 CLIMATE REPRESENTATIVENESS OF 2018

Figures 4.1 and 4.2 show the divisional rankings for observed temperatures across the US for 2018. A climatic representation of the precipitation for 2018 is shown in Figures 4.3 and 4.4. These types of plots are used to determine whether the meteorological conditions in a specific year are near-normal or anomalous. Additionally, we can make determinations of their suitability for use in photochemical modeling in terms of a specific year's conduciveness for photochemical production of secondary pollutants.

In 2018, temperatures were average to much above average, particularly in the late Spring and Summer months. Record or near-record warmth was observed in the Southeast during February, the Central US, Southern Plains, and Mid-Atlantic states during May, as well as in the

Northeast during August and September. Conversely, abnormally cool conditions were observed in the central US during April and September.

With regards to precipitation, 2018 was primarily slightly below to slightly above average across the country. Overall, this would appear to be a near-normal climatology for precipitation. Notably, February and September were wetter than usual in the central and eastern US.

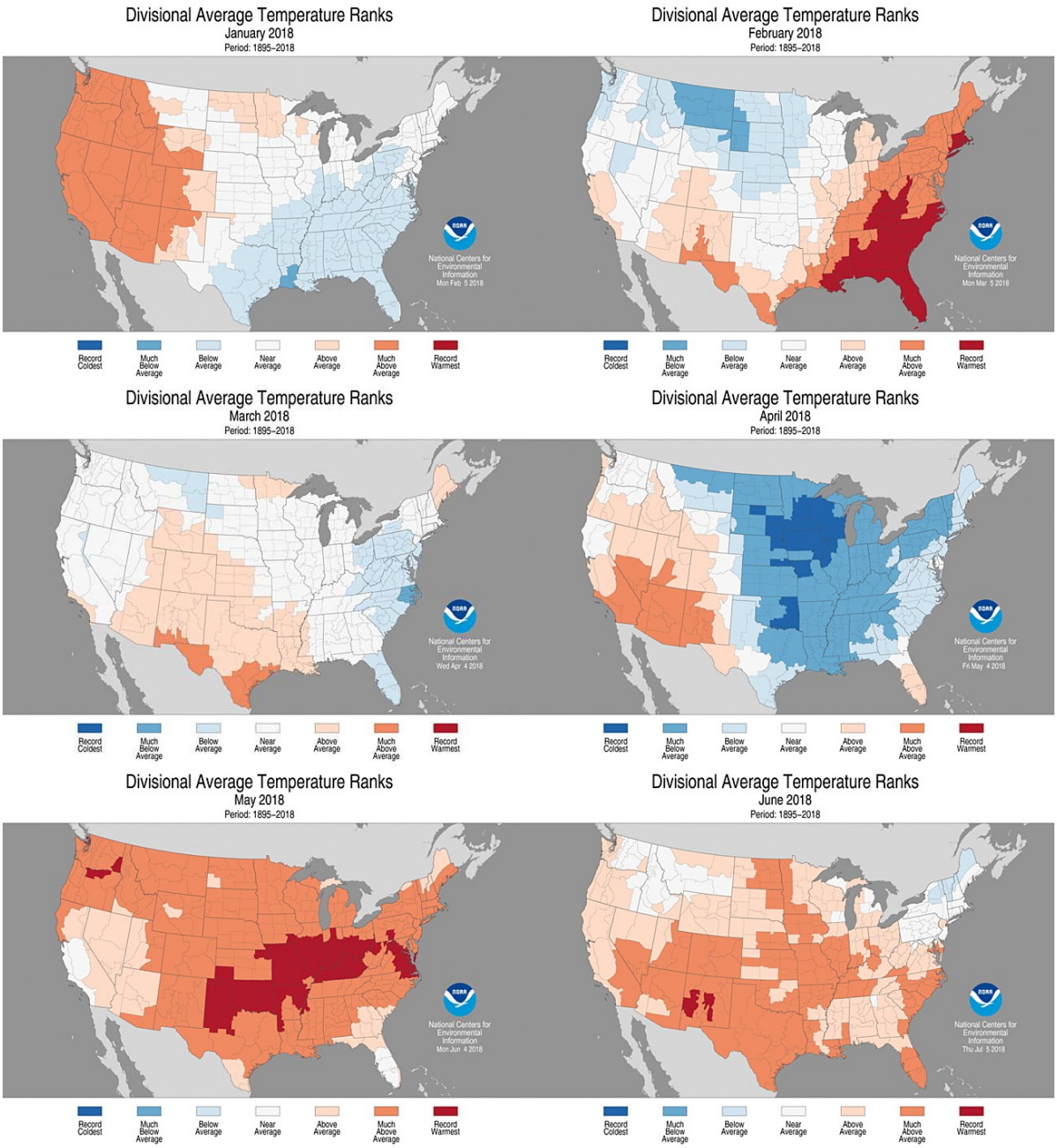

Figure 4.1 Climatic temperature rankings by climate division: January to June 2018. http://www.ncdc.noaa.gov/temp-and-precip/maps.php

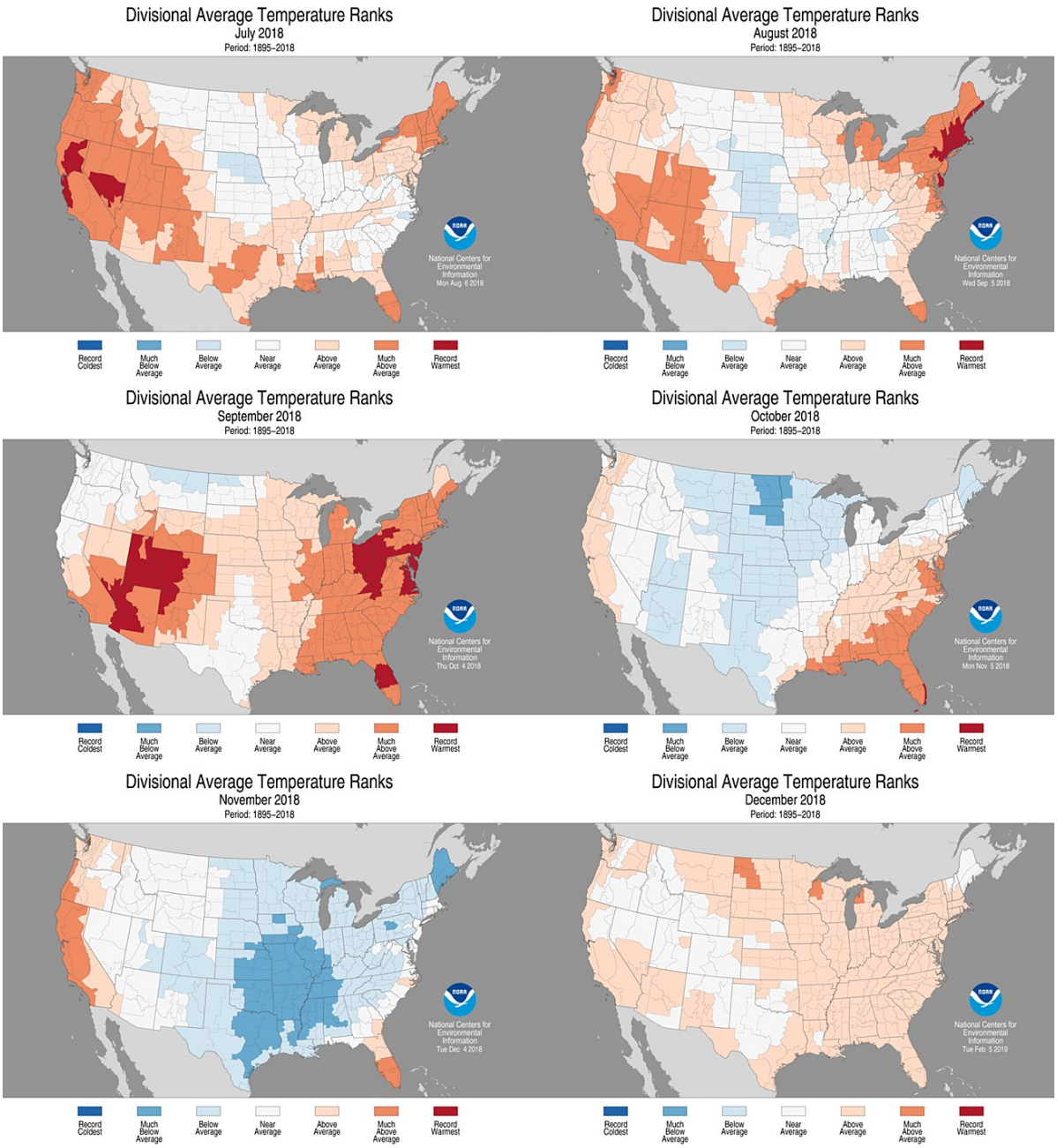

Figure 4.2 Climatic temperature rankings by climate division: July to December 2018. http://www.ncdc.noaa.gov/temp-and-precip/maps.php

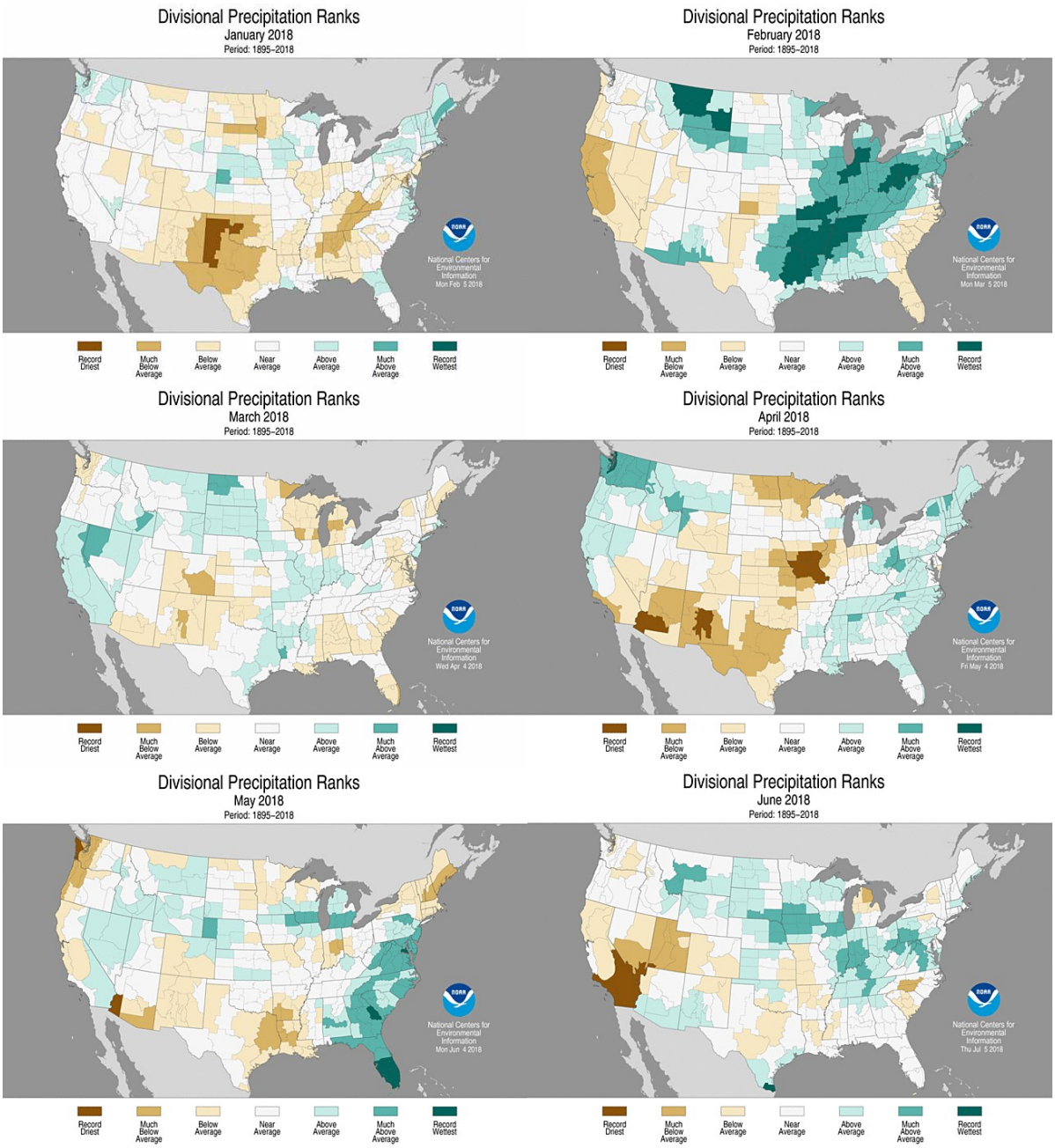

Figure 4.3 Climatic rainfall rankings by climate division: January to June 2018. http://www.ncdc.noaa.gov/temp-and-precip/maps.php

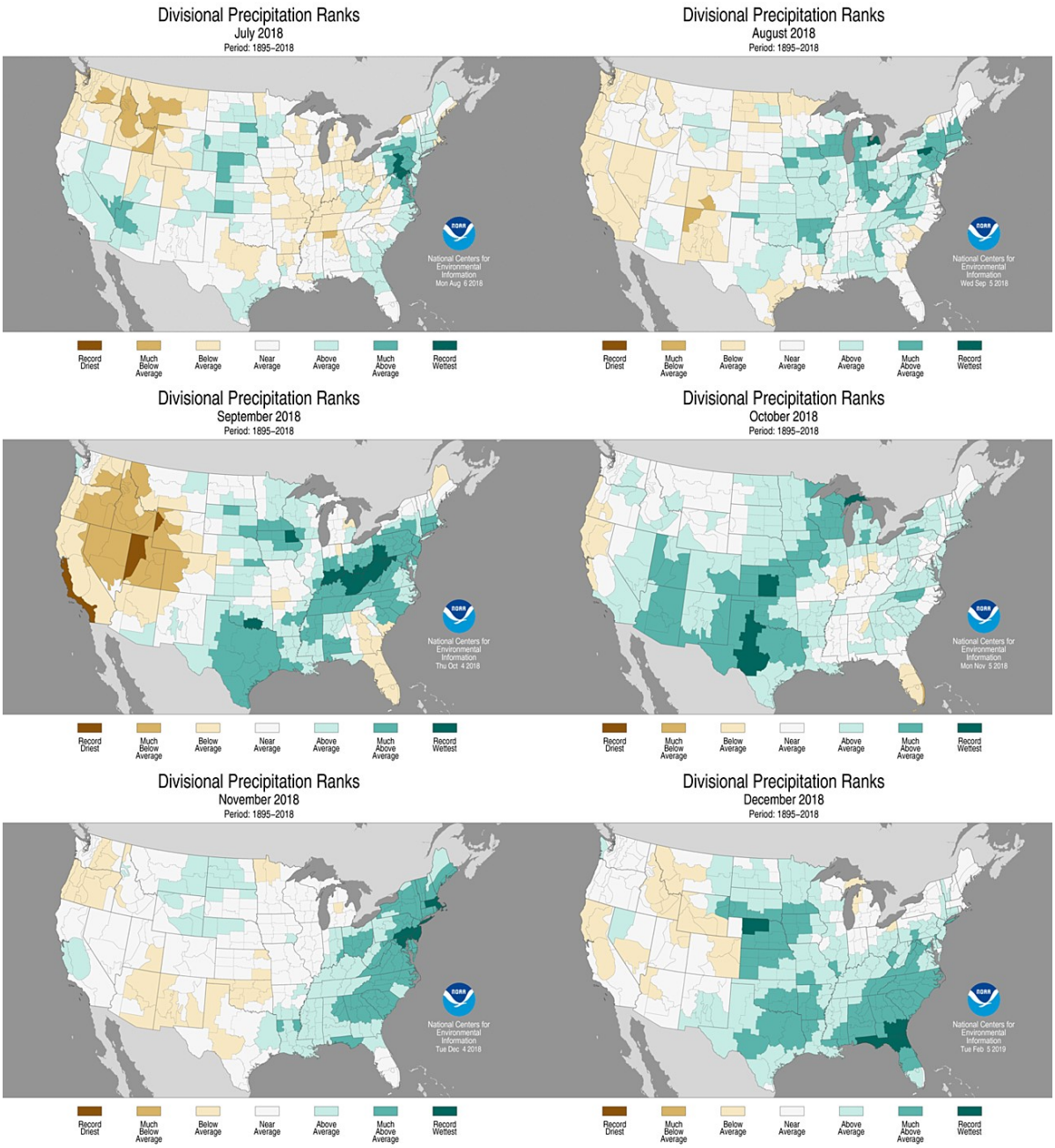

Figure 4.4 Climatic rainfall rankings by climate division: July to December 2018. https://www.ncdc.noaa.gov/sotc/

5 REFERENCES

Boylan, J.W., Russell, A.G., 2006. PM and light extinction model performance metrics, goals, and criteria for three-dimensional air quality models. Atmospheric Environment 40, 4946-4959.

Carlton, A.G., Baker, K.R., 2011. Photochemical Modeling of the Ozark Isoprene Volcano: MEGAN, BEIS, and Their Impacts on Air Quality Predictions. Environmental Science & Technology 45, 4438-4445.

Cooper, O.R., Stohl, A., Hubler, G., Hsie, E.Y., Parrish, D.D., Tuck, A.F., Kiladis, G.N., Oltmans, S.J., Johnson, B.J., Shapiro, M., Moody, J.L., Lefohn, A.S., 2005. Direct Transport of Midlatitude Stratospheric Ozone into the Lower Troposphere and Marine Boundary Layer of the Pacific Ocean. Journal of Geophysical Research – Atmospheres 110, D23310, doi:10.1029/2005JD005783.

ENVIRON, 2008. User's Guide Comprehensive Air Quality Model with Extensions. ENVIRON International Corporation, Novato.

Gilliam, R.C., Pleim, J.E., 2010. Performance Assessment of New Land Surface and Planetary Boundary Layer Physics in the WRF-ARW. Journal of Applied Meteorology and Climatology 49, 760-774.

Heath, Nicholas K., Pleim, J.E., Gilliam, R., Kang, D., 2016. A simple lightning assimilation technique for improving retrospective WRF simulations. Journal of Advances in Modeling Earth Systems. 8. 10.1002/2016MS000735.

Langford, A.O., Reid, S.J., 1998. Dissipation and Mixing of a Small-Scale Stratospheric Intrusion in the Upper Troposphere. Journal of Geophysical Research 103, 31265-31276.

Otte, T.L., Pleim, J.E., 2010. The Meteorology-Chemistry Interface Processor (MCIP) for the CMAQ modeling system: updates through MCIPv3.4.1. Geoscientific Model Development 3, 243-256.

Skamarock, W.C., Klemp, J.B., Dudhia, J., Gill, D.O., Barker, D.M., Duda, M.G., Huang, X., Wang, W., Powers, J.G., 2008. A Description of the Advanced Research WRF Version 3.

Stammer, D., F.J. Wentz, and C.L. Gentemann, 2003, Validation of Microwave Sea Surface Temperature Measurements for Climate Purposes, *J. Climate,* 16, 73-87.

United States Environmental Protection Agency	Office of Air Quality Planning and Standards Air Quality Assessment Division Research Triangle Park, NC	Publication No. EPA-454/R-23-006 July 2023